

Dynamic stiffness matrix based on the extended separation-of-variables solution for the free vibration of orthotropic rectangular thin plates

Shiyi Mei^a, Colin Caprani^{a,*}, Daniel Cantero^b

^a*Department of Civil Engineering, Monash University, Melbourne, Victoria, Australia*

^b*Department of Structural Engineering, Norwegian University of Science & Technology NTNU, Trondheim, Norway*

Abstract

The dynamic stiffness matrix (DSM) based on the extended separation-of-variables (SOV) type mode solution is developed for the free vibration analysis of an orthotropic rectangular thin plate with general homogeneous boundary conditions. The method combines the advantages of the DSM method and the SOV method. The SOV type solution satisfies the governing differential equation derived from Rayleigh's principle and is used to formulate dynamic stiffness matrices. Owing to the characteristics of the SOV type solution, the fully clamped boundary condition problem associated with the Wittrick–Williams algorithm is resolved. The enhanced algorithm is further proposed to solve dynamic stiffness matrices, rather than solving eigenvalue equations. A numerical technique for mode shape computation is also introduced. The accuracy of the proposed method is validated through numerical experiments.

1. Introduction

Rectangular plates play an important role in various engineering fields, including civil, mechanical, and aerospace engineering [3]. The free vibration of plates has been a fundamental research problem for over two centuries.

*Corresponding author

Email addresses: `shiyi.mei1@monash.edu` (Shiyi Mei), `colin.caprani@monash.edu` (Colin Caprani), `daniel.cantero@ntnu.no` (Daniel Cantero)

5 The earliest exact solutions for this problem are the Navier [21] and Levy
6 [14] solutions, which require at least one pair of opposite edges to be simply
7 supported or guided. To solve problems with other boundary conditions, ap-
8 proximate solutions such as the Rayleigh–Ritz method [13] and the Galerkin
9 method [12] have been widely applied. For these approximation methods,
10 beam functions, polynomials, trigonometric functions, and their combina-
11 tions [16] are commonly used as the assumed approximate functions. The
12 accuracy of these solutions depends on how well the assumed approximate
13 functions represent the displacement of the plate.

14 Besides the approximation methods, several analytical methods have been
15 developed over past decades, including the Kantorovich-Krylov method [9,
16 10], the symplectic eigenfunction expansion method [32, 25], the separation-
17 of-variable (SOV) method [29], the dynamic stiffness matrix (DSM) method
18 [2], and series expansion-based methods [24]. The series expansion-based
19 methods include the superposition method [22, 7], Fourier series method
20 [11, 17], the finite integral transform method [15, 33], and other series meth-
21 ods. These methods represent the plate displacement in terms of an infinite
22 series and mostly are capable of handling any general boundary conditions.
23 However, sufficient truncation of the series is required to ensure the accuracy
24 and convergence of the results, and the eigenvalue equation is generally dif-
25 ficult to express explicitly. Therefore, solving the corresponding eigenvalue
26 problem can be computationally expensive.

27 Despite being a powerful method for the dynamic analysis of plate as-
28 semblies, the finite element method (FEM) requires a sufficient number of
29 elements and is computationally expensive to accurately capture higher-order
30 modes. Thus, the DSM method was developed as an accurate and efficient
31 analytical approach to alternatively solve complex plate structures [4, 5]. The
32 DSM can be considered as an analytical FEM since the mode functions of
33 the plate are expressed by analytical solutions, where Levy-type solution [6]
34 or components of infinite Fourier series [1, 19] are applied. To avoid solving
35 the cumbersome transcendental frequency equation directly, the Wittrick-
36 Williams (W-W) algorithm [23] is applied to the eigenvalue problem. The
37 W-W algorithm determines the lower and upper bounds of natural frequen-
38 cies to arbitrary precision rather than solving the frequency equation directly.
39 Thus, the DSM has the potential to be effectively and systematically solved
40 using the W-W algorithm. However, a critical part in applying the W-W
41 algorithm is to determine all natural frequencies of the fully clamped struc-
42 ture within the interested frequency range, *a priori*. Strategies such as using

a sufficiently fine mesh or including a sufficient number of terms in series expansions [1] can ensure that all fully clamped frequencies are accounted for, thereby maintaining the accuracy of the algorithm. However, these approaches are computationally expensive and complex, posing a significant obstacle to the wider adoption and application of the DSM method based on the W-W algorithm [8]. To resolve the fully clamped plate problem, Liu and Banerjee [18] suggested that the frequencies can be indirectly obtained from the simply supported plate problem, where the Navier solution serves as the analytical solution. This provides a significant enhancement to the W-W algorithm, increasing the efficiency of applying DSM methods. However, the solutions are not explicit and closed-form, but are expressed in an infinite series form, where a sufficient number of truncation terms is required to ensure accuracy.

Inspired by the Navier and Levy solutions, Xing and Liu [29] proposed the SOV method, which provides concise and explicit eigensolutions. The mode shape function has a separable form, $\phi(x)\psi(y)$, requiring only one $\phi(x)$ and one $\psi(y)$ for each mode order, allowing each eigenvalue equation to be explicitly expressed. However, this SOV method is not suitable to deal with plates with free boundary conditions. Therefore, an extended SOV method [26, 27] based on the Rayleigh quotient was proposed to accommodate plates with all four classical boundary conditions, i.e., simply supported, clamped, guided, and free. Based on the Rayleigh quotient model, alternative iterative and improved SOV methods have been subsequently proposed [28]. Although SOV methods provide concise closed-form analytical solutions, they require solving a specific set of highly nonlinear eigenvalue equations for each type of boundary condition. However, even when considering only the four classic homogeneous cases, it becomes evident that 55 different boundary condition combinations exist for a rectangular plate, making the process tedious.

In this study, the SOV method is further extended to analyze the vibrations of plates with elastically restrained edges. This extended SOV solution is then employed to construct the dynamic stiffness matrices, which accommodate all general homogeneous boundary conditions. By taking advantage of both the SOV and DSM methods, an enhanced W-W algorithm is developed to solve the eigenvalue problem without directly solving the eigenvalue equations. This enhanced approach resolves the challenge of determining fully clamped frequencies, a well-known limitation in the application of the W-W algorithm. In addition, a novel numerical technique is proposed to compute the mode shape coefficients.

81 2. Mathematical model

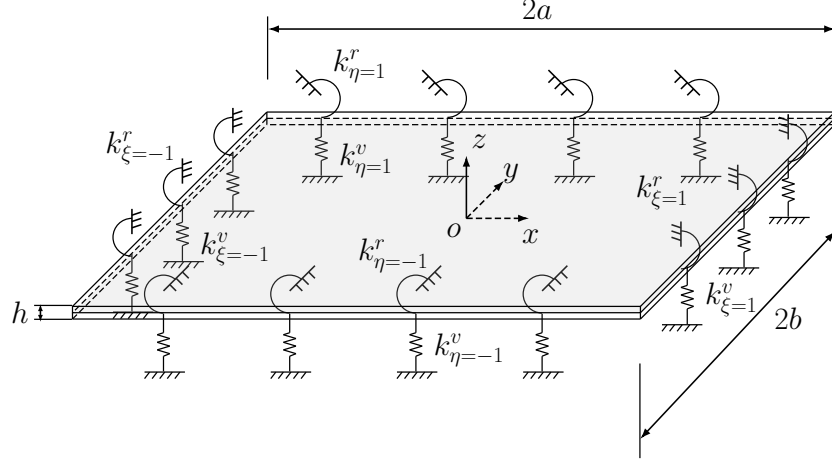


Figure 1: The orthotropic rectangular plate with all edges elastically restrained.

82 Consider a thin orthotropic rectangular plate of length $2a$ and width
 83 $2b$, with all four edges restrained by vertical translational springs k^v and
 84 rotational springs k^r , as shown in Figure 1. The coordinate origin is located
 85 at the center of the plate.

86 The governing differential equation for the free vibration of a thin or-
 87 thotropic plate is given by [28]:

$$D_{11} \frac{\partial^4 w}{\partial \xi^4} + 2D_3 \alpha^2 \frac{\partial^4 w}{\partial \xi^2 \partial \eta^2} + D_{22} \alpha^4 \frac{\partial^4 w}{\partial \eta^4} = \rho h \alpha^4 \omega^2 w, \quad (1)$$

88 where $\alpha = a/b$ is the aspect ratio; $\xi = x/a$ and $\eta = y/b$ are the normalized
 89 coordinates, and the bending stiffness parameters are defined as:

$$\begin{aligned} D_{11} &= \frac{E_1 h^3}{12(1 - v_{12}v_{21})}, & D_{22} &= \frac{E_2 h^3}{12(1 - v_{12}v_{21})}, \\ D_{66} &= \frac{G_{12} h^3}{12}, & D_{12} &= v_{12}D_{22} = v_{21}D_{11}, & D_3 &= D_{12} + 2D_{66}, \end{aligned} \quad (2)$$

90 where ρ and h denote the mass density and thickness of the plate, respec-
 91 tively; E_1 and E_2 are the Young's moduli in the x - and y -directions, respec-
 92 tively; G_{12} is the shear modulus, and v_{12} and v_{21} are the Poisson's ratios.

93 Instead of solving the free vibration of the thin orthotropic plate using
 94 Equation (1), it is suggested that the vibration of the thin plate can also be
 95 solved using the Rayleigh quotient variational principle [26]:

$$\delta U_{mag} = \omega^2 \delta T_0, \quad (3)$$

96 where δ denotes variation, U_{mag} is the magnitude of the potential energy of
 97 the plate, and $\omega^2 T_0$ represents the magnitude of the kinetic energy of the
 98 plate. The potential energy of the plate can be expressed as [27]:

$$U^I = \frac{1}{2} \iint \left[D_{11} \left(\frac{\partial^2 W}{\partial x^2} \right)^2 + 2D_{12} \frac{\partial^2 W}{\partial x^2} \frac{\partial^2 W}{\partial y^2} + D_{22} \left(\frac{\partial^2 W}{\partial y^2} \right)^2 \right. \\ \left. + 4D_{66} \left(\frac{\partial^2 W}{\partial x \partial y} \right)^2 \right] dx dy. \quad (4)$$

99 And the kinetic energy is:

$$T = \frac{1}{2} \iint \rho h \left(\frac{\partial W}{\partial t} \right)^2 dx dy. \quad (5)$$

100 Assuming the solution of the deflection $W(x, y; t) = w(x, y)e^{i\omega t}$ for har-
 101 monic plate motion, where $i = \sqrt{-1}$, $w(x, y)$ is the mode shape, and ω is the
 102 radial frequency. By substituting $W(x, y; t) = w(x, y)e^{i\omega t}$ into Equations (4)
 103 and (5) and expressing the system in dimensionless coordinates, we have:

$$U_{mag}^I = \frac{ab}{2} \iint \left[\frac{D_{11}}{a^4} \left(\frac{\partial^2 w}{\partial \xi^2} \right)^2 + \frac{2D_{12}}{a^2 b^2} \frac{\partial^2 w}{\partial \xi^2} \frac{\partial^2 w}{\partial \eta^2} + \frac{D_{22}}{b^4} \left(\frac{\partial^2 w}{\partial \eta^2} \right)^2 \right. \\ \left. + \frac{4D_{66}}{a^2 b^2} \left(\frac{\partial^2 w}{\partial \xi \partial \eta} \right)^2 \right] d\xi d\eta, \quad (6)$$

104 and

$$T = \omega^2 \frac{ab}{2} \rho h \iint w^2 d\xi d\eta = \omega^2 T_0, \quad (7)$$

105 The separable form of the mode shape function $w(\xi, \eta)$ is given by:

$$w(\xi, \eta) = \phi(\xi)\psi(\eta), \quad (8)$$

106 where $\phi(\xi)$ and $\psi(\eta)$ can be expressed as:

$$\phi(\xi) = A_1 \sin(\alpha_1 \xi) + A_2 \cos(\alpha_1 \xi) + A_3 \sinh(\beta_1 \xi) + A_4 \cosh(\beta_1 \xi), \quad (9a)$$

$$\psi(\eta) = B_1 \sin(\alpha_2 \eta) + B_2 \cos(\alpha_2 \eta) + B_3 \sinh(\beta_2 \eta) + B_4 \cosh(\beta_2 \eta). \quad (9b)$$

107 Based on Equation (3), the frequencies ω_x and ω_y , corresponding to the
 108 mode shapes $\phi(\xi)$ and $\psi(\eta)$, respectively, are assumed to be independent of
 109 each other.

110 2.1. Dynamic stiffness matrix corresponding to ω_x

111 For given general homogeneous boundary conditions, we can first assume
 112 that the mode shape $\psi(\eta)$ corresponding to the y -direction is known. Sup-
 113 posing the edges of the plate in both the x - and y -directions are elastically
 114 restrained by homogeneous vertical translational and rotational springs. The
 115 vertical translational and rotational springs at the $\xi = -1$ end are denoted
 116 as $k_{\xi=-1}^v$ and $k_{\xi=-1}^r$, respectively, and at the $\xi = 1$ end as $k_{\xi=1}^v$ and $k_{\xi=1}^r$,
 117 respectively. Thus, the potential energy along the supported edge in the
 118 x -direction can be expressed by:

$$\begin{aligned} U^{II} = & \int \left[k_{\xi=-1}^r \left(\frac{\partial W}{\partial x} \right)^2 + k_{\xi=-1}^v (W)^2 \right]_{x=-a} dy \\ & + \int \left[k_{\xi=1}^r \left(\frac{\partial W}{\partial x} \right)^2 + k_{\xi=1}^v (W)^2 \right]_{x=a} dy. \end{aligned} \quad (10)$$

119 From Equation (10), the magnitude of total potential energy along the edges
 120 in the x -direction is obtained as:

$$\begin{aligned} U_{mag}^{II} = & ab \int \left[\frac{k_{\xi=-1}^r}{a^3} \left(\frac{\partial w}{\partial \xi} \right)^2 + \frac{k_{\xi=-1}^v}{a} (w)^2 \right]_{\xi=-1} d\eta \\ & + ab \int \left[\frac{k_{\xi=1}^r}{a^3} \left(\frac{\partial w}{\partial \xi} \right)^2 + \frac{k_{\xi=1}^v}{a} (w)^2 \right]_{\xi=1} d\eta. \end{aligned} \quad (11)$$

121 The magnitude of potential energy of the plate in the x -direction can be
 122 obtained from Equations (6) and (11) as:

$$\begin{aligned}
 U_{mag} &= U_{mag}^I + U_{mag}^{II} \\
 &= \frac{ab}{2} \iint \left[\frac{D_{11}}{a^4} \left(\frac{\partial^2 w}{\partial \xi^2} \right)^2 + \frac{2D_{12}}{a^2 b^2} \frac{\partial^2 w}{\partial \xi^2} \frac{\partial^2 w}{\partial \eta^2} + \frac{D_{22}}{b^4} \left(\frac{\partial^2 w}{\partial \eta^2} \right)^2 \right. \\
 &\quad \left. + \frac{4D_{66}}{a^2 b^2} \left(\frac{\partial^2 w}{\partial \xi \partial \eta} \right)^2 \right] d\xi d\eta \\
 &\quad + ab \int \left[\frac{k_{\xi=1}^r}{a^3} \left(\frac{\partial w}{\partial \xi} \right)^2 + \frac{k_{\xi=1}^v}{a} (w)^2 \right]_{\xi=1} d\eta \\
 &\quad + ab \int \left[\frac{k_{\xi=-1}^r}{a^3} \left(\frac{\partial w}{\partial \xi} \right)^2 + \frac{k_{\xi=-1}^v}{a} (w)^2 \right]_{\xi=-1} d\eta
 \end{aligned} \tag{12}$$

123 By substituting Equation (8) into Equation (12), we have:

$$\begin{aligned}
 U_{mag} &= \frac{ab}{2} \int_{-1}^1 \left[\frac{D_{11}}{a^4} I_1 \left(\frac{d^2 \phi}{d\xi^2} \right)^2 + \frac{2D_{12}}{a^2 b^2} I_2 \frac{d^2 \phi}{d\xi^2} \phi + \frac{D_{22}}{b^4} I_4 \phi^2 \right. \\
 &\quad \left. + \frac{4D_{66}}{a^2 b^2} I_3 \left(\frac{d\phi}{d\xi} \right)^2 \right] d\xi \\
 &\quad + ab I_1 \left[\frac{k_{\xi=-1}^r}{a^3} \left(\frac{d\phi}{d\xi} \right)^2 + \frac{k_{\xi=-1}^v}{a} (\phi)^2 \right]_{\xi=-1} \\
 &\quad + ab I_1 \left[\frac{k_{\xi=1}^r}{a^3} \left(\frac{d\phi}{d\xi} \right)^2 + \frac{k_{\xi=1}^v}{a} (\phi)^2 \right]_{\xi=1},
 \end{aligned} \tag{13}$$

124 where the integral parameters are defined as:

$$\begin{aligned}
 I_1 &= \int_{-1}^1 \psi^2 d\eta, \\
 I_2 &= \int_{-1}^1 \left(\frac{d^2 \psi}{d\eta^2} \psi \right) d\eta, \\
 I_3 &= \int_{-1}^1 \left(\frac{d\psi}{d\eta} \right)^2 d\eta, \\
 I_4 &= \int_{-1}^1 \left(\frac{d^2 \psi}{d\eta^2} \right)^2 d\eta.
 \end{aligned} \tag{14}$$

125 By taking Equation (8) into account, the coefficient T_0 of the kinetic energy
 126 from Equation (7) for the plate can be expressed as:

$$T_0 = \frac{ab}{2} \rho h \iint w^2 d\xi d\eta = \frac{ab}{2} \rho h I_1 \int_{-1}^1 \phi^2 d\xi. \quad (15)$$

127 Taking the Rayleigh principle in the form:

$$\delta U_{mag} = \omega_x^2 \delta T_0, \quad (16)$$

128 and by substituting Equations (13) and (15) into Equation (16), and relieving
 129 $\delta\phi$ and $\delta \frac{d\phi}{d\xi}$ in Equation (16) by calculus of variations, yields:

$$\begin{aligned} 0 = & \int_{-1}^1 \left[\frac{D_{11}}{a^4} I_1 \frac{d^4\phi}{d\xi^4} + \left(\frac{2D_{12}}{a^2b^2} I_2 - \frac{4D_{66}}{a^2b^2} I_3 \right) \frac{d^2\phi}{d\xi^2} \right. \\ & + \left. \left(\frac{D_{22}}{b^4} I_4 - \omega_x^2 \rho h I_1 \right) \phi \right] \delta\phi d\xi \\ & + \frac{2k_{\xi=-1}^v}{a} I_1 (\phi \delta\phi)_{\xi=-1} + \frac{2k_{\xi=1}^v}{a} I_1 (\phi \delta\phi)_{\xi=1} \\ & + \left[\left(\frac{4D_{66}}{a^2b^2} I_3 - \frac{D_{12}}{a^2b^2} I_2 \right) \frac{d\phi}{d\xi} - \frac{D_{11}}{a^4} I_1 \frac{d^3\phi}{d\xi^3} \right] \delta\phi \Big|_{\xi=-1}^{\xi=1} \\ & + \left(\frac{D_{12}}{a^2b^2} I_2 \phi + \frac{D_{11}}{a^4} I_1 \frac{d^2\phi}{d\xi^2} \right) \delta \frac{d\phi}{d\xi} \Big|_{\xi=-1}^{\xi=1} \\ & + \frac{2k_{\xi=-1}^r}{a^3} I_1 \left(\frac{d\phi}{d\xi} \delta \frac{d\phi}{d\xi} \right)_{\xi=-1} + \frac{2k_{\xi=1}^r}{a^3} I_1 \left(\frac{d\phi}{d\xi} \delta \frac{d\phi}{d\xi} \right)_{\xi=1}. \end{aligned} \quad (17)$$

130 Thus, the governing differential equation in the x -direction can be obtained
 131 from the integration part in Equation (17):

$$\frac{d^4\phi}{d\xi^4} + 2\alpha^2 \left(\frac{D_{12}I_2}{D_{11}I_1} - 2\frac{D_{66}I_3}{D_{11}I_1} \right) \frac{d^2\phi}{d\xi^2} + \left(\alpha^4 \frac{D_{22}I_4}{D_{11}I_1} - a^4 \Omega_x^4 \right) \phi = 0, \quad (18)$$

132 where $\Omega_x = \sqrt[4]{\omega_x^2 \rho h / D_{11}}$. By substituting $\phi(\xi) = Ae^{\mu\xi}$ into Equation (18),
 133 we obtain:

$$\mu^4 + 2\alpha^2 \left(\frac{D_{12}I_2}{D_{11}I_1} - 2\frac{D_{66}I_3}{D_{11}I_1} \right) \mu^2 + \left(\alpha^4 \frac{D_{22}I_4}{D_{11}I_1} - a^4 \Omega_x^4 \right) = 0. \quad (19)$$

134 And so the solution for μ can be expressed as:

$$\mu_{1,2} = \pm i\alpha_1, \quad \mu_{3,4} = \pm \beta_1, \quad (20)$$

135 where,

$$\alpha_1 = \alpha \sqrt{\sqrt{\left(\frac{D_{12}I_2}{D_{11}I_1} - 2\frac{D_{66}I_3}{D_{11}I_1}\right)^2 - \frac{D_{22}I_4}{D_{11}I_1} + b^4\Omega_x^4} + \frac{D_{12}I_2}{D_{11}I_1} - 2\frac{D_{66}I_3}{D_{11}I_1}}, \quad (21a)$$

$$\beta_1 = \alpha \sqrt{\sqrt{\left(\frac{D_{12}I_2}{D_{11}I_1} - 2\frac{D_{66}I_3}{D_{11}I_1}\right)^2 - \frac{D_{22}I_4}{D_{11}I_1} + b^4\Omega_x^4} - \frac{D_{12}I_2}{D_{11}I_1} + 2\frac{D_{66}I_3}{D_{11}I_1}}. \quad (21b)$$

136 The boundary conditions along the edges in the x -direction can be obtained
 137 from the remaining $\delta\phi$ and $\delta\frac{d\phi}{d\xi}$ parts in Equation (17). The shear force
 138 equilibrium can be obtained from the $\delta\phi$ part:

$$\begin{aligned} & \left[\left(\frac{4D_{66}}{a^2b^2}I_3 - \frac{D_{12}}{a^2b^2}I_2 \right) \frac{d\phi}{d\xi} - \frac{D_{11}}{a^4}I_1 \frac{d^3\phi}{d\xi^3} \right] \Big|_{\xi=-1}^{\xi=1} \\ & + \frac{2k_{\xi=-1}^v}{a}I_1(\phi)_{\xi=-1} + \frac{2k_{\xi=1}^v}{a}I_1(\phi)_{\xi=1} = 0, \end{aligned} \quad (22)$$

139 and from the $\delta\frac{d\phi}{d\xi}$ part, the bending moment equilibrium:

$$\begin{aligned} & \left(\frac{D_{12}}{a^2b^2}I_2\phi + \frac{D_{11}}{a^4}I_1 \frac{\partial^2\phi}{\partial\xi^2} \right) \Big|_{\xi=-1}^{\xi=1} \\ & + \frac{2k_{\xi=-1}^r}{a^3}I_1 \left(\frac{\partial\phi}{\partial\xi} \right)_{\xi=-1} + \frac{2k_{\xi=1}^r}{a^3}I_1 \left(\frac{\partial\phi}{\partial\xi} \right)_{\xi=1} = 0. \end{aligned} \quad (23)$$

140 Thus, we can obtain the shear force and bending moment equilibrium along
 141 the edges $\xi = -1$ and $\xi = 1$ from Equations (22) and (23), respectively, as:

$$\frac{d^3\phi}{d\xi^3} - \alpha^2 \left(\frac{4D_{66}I_3}{D_{11}I_1} - \frac{D_{12}I_2}{D_{11}I_1} \right) \frac{d\phi}{d\xi} + \frac{2a^3k_{\xi=-1}^v}{D_{11}}\phi = 0, \quad \xi = -1, \quad (24a)$$

$$\frac{d^2\phi}{d\xi^2} + \frac{\alpha^2 D_{12}I_2}{D_{11}I_1}\phi - \frac{2ak_{\xi=-1}^r}{D_{11}} \frac{d\phi}{d\xi} = 0, \quad \xi = -1, \quad (24b)$$

$$\frac{d^3\phi}{d\xi^3} - \alpha^2 \left(\frac{4D_{66}I_3}{D_{11}I_1} - \frac{D_{12}I_2}{D_{11}I_1} \right) \frac{d\phi}{d\xi} - \frac{2a^3k_{\xi=1}^v}{D_{11}}\phi = 0, \quad \xi = 1, \quad (24c)$$

$$\frac{d^2\phi}{d\xi^2} + \frac{\alpha^2 D_{12}I_2}{D_{11}I_1}\phi + \frac{2ak_{\xi=1}^r}{D_{11}} \frac{d\phi}{d\xi} = 0, \quad \xi = 1. \quad (24d)$$

142 Substituting Equation (9a) into Equation (24), and denoting $k_\xi^{u*} \equiv \frac{2a^3 k_\xi^u}{D_{11}}$ for
 143 $u \in \{r, v\}$, $S_u \equiv \sin u$, $C_u \equiv \cos u$, $Sh_u \equiv \sinh u$, and $Ch_u \equiv \cosh u$, we have:

$$\begin{bmatrix} \gamma_1 C_{\alpha_1} - k_{\xi=-1}^{v*} S_{\alpha_1} & \gamma_1 S_{\alpha_1} + k_{\xi=-1}^{v*} C_{\alpha_1} & \gamma_2 Ch_{\beta_1} - k_{\xi=-1}^{v*} Sh_{\beta_1} \\ \gamma_3 S_{\alpha_1} + k_{\xi=-1}^{r*} \alpha_1 C_{\alpha_1} & -\gamma_3 C_{\alpha_1} + k_{\xi=-1}^{r*} \alpha_1 S_{\alpha_1} & \gamma_4 Sh_{\beta_1} + k_{\xi=-1}^{r*} \beta_1 Ch_{\beta_1} \\ -\gamma_1 C_{\alpha_1} + k_{\xi=1}^{v*} S_{\alpha_1} & \gamma_1 S_{\alpha_1} + k_{\xi=1}^{v*} C_{\alpha_1} & -\gamma_2 Ch_{\beta_1} + k_{\xi=1}^{v*} Sh_{\beta_1} \\ \gamma_3 S_{\alpha_1} + k_{\xi=1}^{r*} \alpha_1 C_{\alpha_1} & \gamma_3 C_{\alpha_1} - k_{\xi=1}^{r*} \alpha_1 S_{\alpha_1} & \gamma_4 Sh_{\beta_1} + k_{\xi=1}^{r*} \beta_1 Ch_{\beta_1} \\ -\gamma_2 Sh_{\beta_1} + k_{\xi=-1}^{v*} Ch_{\beta_1} \\ -\gamma_4 Ch_{\beta_1} - k_{\xi=-1}^{r*} \beta_1 Sh_{\beta_1} \\ -\gamma_2 Sh_{\beta_1} + k_{\xi=1}^{v*} Ch_{\beta_1} \\ \gamma_4 Ch_{\beta_1} + k_{\xi=1}^{r*} \beta_1 Sh_{\beta_1} \end{bmatrix} \begin{Bmatrix} A_1 \\ A_2 \\ A_3 \\ A_4 \end{Bmatrix} = \begin{Bmatrix} 0 \\ 0 \\ 0 \\ 0 \end{Bmatrix}, \quad (25)$$

144 OR,

$$\mathbf{R}_x \mathbf{A} = \mathbf{0}, \quad (26)$$

145 where,

$$\begin{aligned} \gamma_1 &= -\alpha_1^3 - \alpha^2 \left(\frac{4D_{66}S_3}{D_{11}I_1} - \frac{D_{12}I_2}{D_{11}I_1} \right) \alpha_1, \\ \gamma_2 &= \beta_1^3 - \alpha^2 \left(\frac{4D_{66}S_3}{D_{11}I_1} - \frac{D_{12}I_2}{D_{11}I_1} \right) \beta_1, \\ \gamma_3 &= -\alpha_1^2 + \frac{\alpha^2 D_{12}I_2}{D_{11}I_1}, \\ \gamma_4 &= \beta_1^2 + \frac{\alpha^2 D_{12}I_2}{D_{11}I_1}. \end{aligned} \quad (27)$$

146 Note that the classic boundary conditions can be obtained by selecting ex-
 147 tremely large or small spring stiffness constants. For non-trivial solutions,
 148 the characteristic equation or eigenvalue equation is obtained from the de-
 149 terminant of the matrix \mathbf{R}_x in Equation (26), which must be zero. However,
 150 solving these transcendental equations is cumbersome and so the DSM is
 151 introduced to avoid such a computation.

152 To develop the plate's dynamic stiffness matrix, with the help of Equa-
 153 tion (9a), the vertical displacement and rotation corresponding to the mode
 154 shape $\phi(\xi)$ along the x -direction at edges $\xi = -1$ and $\xi = 1$ can be expressed
 155 as:

$$\begin{Bmatrix} \phi_{\xi=-1} \\ \frac{d\phi}{d\xi}_{\xi=-1} \\ \phi_{\xi=1} \\ \frac{d\phi}{d\xi}_{\xi=1} \end{Bmatrix} = \begin{bmatrix} -S_{\alpha_1} & C_{\alpha_1} & -Sh_{\beta_1} & Ch_{\beta_1} \\ \alpha_1 C_{\alpha_1}/a & \alpha_1 S_{\alpha_1}/a & \beta_1 Ch_{\beta_1}/a & -\beta_1 Sh_{\beta_1}/a \\ S_{\alpha_1} & C_{\alpha_1} & Sh_{\beta_1} & Ch_{\beta_1} \\ \alpha_1 C_{\alpha_1}/a & -\alpha_1 S_{\alpha_1}/a & \beta_1 Ch_{\beta_1}/a & \beta_1 Sh_{\beta_1}/a \end{bmatrix} \begin{Bmatrix} A_1 \\ A_2 \\ A_3 \\ A_4 \end{Bmatrix}, \quad (28)$$

156 or,

$$\delta_x = \mathbf{Q}_x \mathbf{A}. \quad (29)$$

157 Solving for the eigenvector \mathbf{A} , and then substituting into Equation (26), we
158 obtain:

$$\mathbf{R}_x \mathbf{A} = \mathbf{R}_x \mathbf{Q}_x^{-1} \delta_x = \mathbf{0}. \quad (30)$$

159 where the dynamic stiffness matrix, denoted as $\mathbf{K}_x = \mathbf{R}_x \mathbf{Q}_x^{-1}$, can be ob-
160 tained from Equation (30). This matrix can be used to compute the natural
161 frequencies of the system instead of solving the eigenvalue equation, and the
162 method for the computation will be given in Section 3.

163 2.2. Dynamic stiffness matrix corresponding to ω_y

164 In this section, the mode shape $\phi(\xi)$ derived in *Section 2.1* is utilized to
165 obtain the dynamic stiffness matrix in the y -direction. The vertical trans-
166 lational and rotational springs at $\eta = -1$ are denoted as $k_{\eta=-1}^v$ and $k_{\eta=-1}^r$,
167 respectively, while those at $\eta = 1$ are represented by $k_{\eta=1}^v$ and $k_{\eta=1}^r$.

168 The magnitude of total potential energy along the edges in the y -direction
169 is given by:

$$\begin{aligned} U_{mag}^{III} = & ab \int \left[\frac{k_{\eta=-1}^r}{a^3} \left(\frac{\partial w}{\partial \eta} \right)^2 + \frac{k_{\eta=-1}^v}{a} w^2 \right]_{\eta=-1} d\xi \\ & + ab \int \left[\frac{k_{\eta=1}^r}{a^3} \left(\frac{\partial w}{\partial \eta} \right)^2 + \frac{k_{\eta=1}^v}{a} w^2 \right]_{\eta=1} d\xi. \end{aligned} \quad (31)$$

170 The magnitude of potential energy of the plate in the y -direction can be
171 obtained from Equations (6) and (31) as:

$$\begin{aligned} U_{mag} = & U_{mag}^I + U_{mag}^{III} \\ = & \frac{ab}{2} \iint \left[\frac{D_{11}}{a^4} \left(\frac{\partial^2 w}{\partial \xi^2} \right)^2 + \frac{2D_{12}}{a^2 b^2} \frac{\partial^2 w}{\partial \xi^2} \frac{\partial^2 w}{\partial \eta^2} + \frac{D_{22}}{b^4} \left(\frac{\partial^2 w}{\partial \eta^2} \right)^2 \right. \\ & \left. + \frac{4D_{66}}{a^2 b^2} \left(\frac{\partial^2 w}{\partial \xi \partial \eta} \right)^2 \right] d\xi d\eta + ab \int \left[\frac{k_{\eta=1}^r}{b^3} \left(\frac{\partial w}{\partial \eta} \right)^2 + \frac{k_{\eta=1}^v}{b} (w)^2 \right]_{\eta=1} d\xi \\ & + ab \int \left[\frac{k_{\eta=-1}^r}{b^3} \left(\frac{\partial w}{\partial \eta} \right)^2 + \frac{k_{\eta=-1}^v}{b} (w)^2 \right]_{\eta=-1} d\xi. \end{aligned} \quad (32)$$

172 By substituting Equation (8) into Equation (32), we obtain:

$$\begin{aligned}
U_{mag} &= U_{mag}^I + U_{mag}^{III} \\
&= \frac{ab}{2} \int_{-1}^1 \left[\frac{D_{11}}{a^4} J_4 \psi^2 + \frac{2D_{12}}{a^2 b^2} J_2 \frac{d^2 \psi}{d\eta^2} \psi + \frac{D_{22}}{b^4} J_1 \left(\frac{d^2 \psi}{d\eta^2} \right)^2 \right. \\
&\quad \left. + \frac{4D_{66}}{a^2 b^2} J_3 \left(\frac{d\psi}{d\eta} \right)^2 \right] d\eta + ab J_1 \left[\frac{k_{\eta=1}^r}{b^3} \left(\frac{d\psi}{d\eta} \right)^2 + \frac{k_{\eta=1}^v}{b} (\psi)^2 \right]_{\eta=1} \\
&\quad + ab J_1 \left[\frac{k_{\eta=-1}^r}{b^3} \left(\frac{d\psi}{d\eta} \right)^2 + \frac{k_{\eta=-1}^v}{b} (\psi)^2 \right]_{\eta=-1}, \tag{33}
\end{aligned}$$

173 where the integral parameters are defined as:

$$\begin{aligned}
J_1 &= \int_{-1}^1 \phi^2 d\xi, \\
J_2 &= \int_{-1}^1 \left(\frac{d^2 \phi}{d\xi^2} \phi \right) d\xi, \\
J_3 &= \int_{-1}^1 \left(\frac{d\phi}{d\xi} \right)^2 d\xi, \\
J_4 &= \int_{-1}^1 \left(\frac{d^2 \phi}{d\xi^2} \right)^2 d\xi. \tag{34}
\end{aligned}$$

174 The coefficient T_0 of the kinetic energy from Equation (7) for the plate can
175 be expressed as:

$$T_0 = \frac{ab}{2} \rho h J_1 \int_{-1}^1 \psi^2 d\eta. \tag{35}$$

176 Take the Rayleigh principle in the form:

$$\delta U_{mag} = \omega_y^2 \delta T_0. \tag{36}$$

177 By substituting Equations (33) and (35) into Equation (36), and relieving

178 $\delta\psi$ and $\delta\frac{d\psi}{d\eta}$ in Equation (36) by variation calculus, yields:

$$\begin{aligned}
0 = & \int_{-1}^1 \left[\frac{D_{22}}{b^4} J_1 \frac{d^4\psi}{d\eta^4} + \left(\frac{2D_{12}}{a^2b^2} J_2 - \frac{4D_{66}}{a^2b^2} J_3 \right) \frac{d^2\psi}{d\eta^2} \right. \\
& + \left. \left(\frac{D_{11}}{a^4} J_4 - \omega_y^2 \rho h J_1 \right) \psi \right] \delta\psi d\eta \\
& + \frac{2k_{\eta=-1}^v}{b} J_1 (\psi \delta\psi)_{\eta=-1} + \frac{2k_{\eta=1}^v}{b} J_1 (\psi \delta\psi)_{\eta=1} \\
& + \left[\left(\frac{4D_{66}}{a^2b^2} J_3 - \frac{D_{12}}{a^2b^2} J_2 \right) \frac{d\psi}{d\eta} - \frac{D_{22}}{b^4} J_1 \frac{d^3\psi}{d\eta^3} \right] \delta\psi \Big|_{\eta=-1}^{\eta=1} \\
& + \left(\frac{D_{12}}{a^2b^2} J_2 \psi + \frac{D_{22}}{b^4} J_1 \frac{d^2\psi}{d\eta^2} \right) \delta \frac{d\psi}{d\eta} \Big|_{\eta=-1}^{\eta=1} \\
& + \frac{2k_{\eta=-1}^r}{b^3} J_1 \left(\frac{d\psi}{d\eta} \delta \frac{d\psi}{d\eta} \right)_{\eta=-1} + \frac{2k_{\eta=1}^r}{b^3} J_1 \left(\frac{d\psi}{d\eta} \delta \frac{d\psi}{d\eta} \right)_{\eta=1}.
\end{aligned} \tag{37}$$

179 Thus, the governing differential equation in the y -direction can be obtained
180 from the integration part in Equation (37):

$$\frac{d^4\psi}{d\eta^4} + \frac{2}{\alpha^2} \left(\frac{D_{12}J_2}{D_{22}J_1} - 2 \frac{D_{66}J_3}{D_{22}J_1} \right) \frac{d^2\psi}{d\eta^2} + \left(\frac{D_{11}J_4}{\alpha^4 D_{22}J_1} - \frac{b^4 D_{11}}{D_{22}} \Omega_y^4 \right) \psi = 0, \tag{38}$$

181 where $\Omega_y = \sqrt[4]{\omega_y^2 \rho h / D_{11}}$. By substituting $\psi(\eta) = Be^{\lambda\eta}$ into Equation (38),
182 yields:

$$\lambda^4 + \frac{2}{\alpha^2} \left(\frac{D_{12}J_2}{D_{22}J_1} - 2 \frac{D_{66}J_3}{D_{22}J_1} \right) \lambda^2 + \left(\frac{D_{11}J_4}{\alpha^4 D_{22}J_1} - \frac{b^4 D_{11}}{D_{22}} \Omega_y^4 \right) = 0. \tag{39}$$

183 The solution for λ can be expressed as:

$$\lambda_{1,2} = \pm i\alpha_2, \quad \lambda_{3,4} = \pm \beta_2, \tag{40}$$

184 where,

$$\alpha_2 = \frac{1}{\alpha} \sqrt{\sqrt{\left(\frac{D_{12}J_2}{D_{22}J_1} - 2 \frac{D_{66}J_3}{D_{22}J_1} \right)^2 - \frac{D_{11}J_4}{D_{22}J_1} + \frac{a^4 D_{11}}{D_{22}} \Omega_y^4} + \frac{D_{12}J_2}{D_{22}J_1} - 2 \frac{D_{66}J_3}{D_{22}J_1}}, \tag{41a}$$

$$\beta_2 = \frac{1}{\alpha} \sqrt{\sqrt{\left(\frac{D_{12}J_2}{D_{22}J_1} - 2 \frac{D_{66}J_3}{D_{22}J_1} \right)^2 - \frac{D_{11}J_4}{D_{22}J_1} + \frac{a^4 D_{11}}{D_{22}} \Omega_y^4} - \frac{D_{12}J_2}{D_{22}J_1} + 2 \frac{D_{66}J_3}{D_{22}J_1}}. \tag{41b}$$

185 The boundary conditions along the edges in the y -direction can be obtained
 186 from the remaining $\delta\psi$ and $\delta\frac{d\psi}{d\eta}$ parts in Equation (37). The shear force
 187 equilibrium can be obtained from the $\delta\psi$ part:

$$\begin{aligned} & \left[\left(\frac{4D_{66}}{a^2b^2} J_3 - \frac{D_{12}}{a^2b^2} J_2 \right) \frac{d\psi}{d\eta} - \frac{D_{22}}{b^4} J_1 \frac{d^3\psi}{d\eta^3} \right] \Big|_{\eta=-1}^{\eta=1} \\ & + \frac{2k_{\eta=-1}^v}{b} J_1(\psi)_{\eta=-1} + \frac{2k_{\eta=1}^v}{b} J_1(\psi)_{\eta=1} = 0, \end{aligned} \quad (42)$$

188 and from the $\delta\frac{d\psi}{d\eta}$ part, the bending moment equilibrium:

$$\begin{aligned} & \left(\frac{D_{12}}{a^2b^2} J_2 \psi + \frac{D_{22}}{b^4} J_1 \frac{d^2\psi}{d\eta^2} \right) \Big|_{\eta=-1}^{\eta=1} + \frac{2k_{\eta=-1}^r}{b^3} J_1 \left(\frac{d\psi}{d\eta} \right)_{\eta=-1} \\ & + \frac{2k_{\eta=1}^r}{b^3} J_1 \left(\frac{d\psi}{d\eta} \right)_{\eta=1} = 0. \end{aligned} \quad (43)$$

189 Thus, we can obtain the shear force and bending moment equilibrium along
 190 the edges $\eta = -1$ and $\eta = 1$ from Equations (42) and (43), respectively, as:

$$\frac{d^3\psi}{d\eta^3} - \left(\frac{4D_{66}J_3}{\alpha^2D_{22}J_1} - \frac{D_{12}J_2}{\alpha^2D_{22}J_1} \right) \frac{d\psi}{d\eta} + \frac{2b^3k_{\eta=-1}^v}{D_{22}} \psi = 0, \quad \eta = -1, \quad (44a)$$

$$\frac{d^2\psi}{d\eta^2} + \frac{D_{12}J_2}{\alpha^2D_{22}J_1} \psi - \frac{2bk_{\eta=-1}^r}{D_{22}} \frac{d\psi}{d\eta} = 0, \quad \eta = -1, \quad (44b)$$

$$\frac{d^3\psi}{d\eta^3} - \left(\frac{4D_{66}J_3}{\alpha^2D_{22}J_1} - \frac{D_{12}J_2}{\alpha^2D_{22}J_1} \right) \frac{d\psi}{d\eta} - \frac{2b^3k_{\eta=1}^v}{D_{22}} \psi = 0, \quad \eta = 1, \quad (44c)$$

$$\frac{d^2\psi}{d\eta^2} + \frac{D_{12}J_2}{\alpha^2D_{22}J_1} \psi + \frac{2bk_{\eta=1}^r}{D_{22}} \frac{d\psi}{d\eta} = 0, \quad \eta = 1. \quad (44d)$$

191 Substituting Equation (9b) into Equation (44) and denoting $k_{\eta}^{v*} = \frac{2b^3k_{\eta}^v}{D_{22}}$,
 192 $k_{\eta}^{r*} = \frac{2bk_{\eta}^r}{D_{22}}$, $S_{\alpha_2} = \sin \alpha_2$, $C_{\alpha_2} = \cos \alpha_2$, $Sh_{\alpha_2} = \sinh \alpha_2$, $Ch_{\alpha_2} = \cosh \alpha_2$,
 193 $S_{\beta_2} = \sin \beta_2$, $C_{\beta_2} = \cos \beta_2$, $Sh_{\beta_2} = \sinh \beta_2$, and $Ch_{\beta_2} = \cosh \beta_2$, We obtain:

$$\begin{aligned} & \begin{bmatrix} \zeta_1 C_{\alpha_2} - k_{\eta=-1}^{v*} S_{\alpha_2} & \zeta_1 S_{\alpha_2} + k_{\eta=-1}^{v*} C_{\alpha_2} & \zeta_2 Ch_{\beta_2} - k_{\eta=-1}^{v*} Sh_{\beta_2} \\ \zeta_3 S_{\alpha_2} + k_{\eta=-1}^{r*} \alpha_2 C_{\alpha_2} & -\zeta_3 C_{\alpha_2} + k_{\eta=-1}^{r*} \alpha_2 S_{\alpha_2} & \zeta_4 Sh_{\beta_2} + k_{\eta=-1}^{r*} \beta_2 Ch_{\beta_2} \\ -\zeta_1 C_{\alpha_2} + k_{\eta=1}^{v*} S_{\alpha_2} & \zeta_1 S_{\alpha_2} + k_{\eta=1}^{v*} C_{\alpha_2} & -\zeta_2 Ch_{\beta_2} + k_{\eta=1}^{v*} Sh_{\beta_2} \\ \zeta_3 S_{\alpha_2} + k_{\eta=1}^{r*} \alpha_2 C_{\alpha_2} & \zeta_3 C_{\alpha_2} - k_{\eta=1}^{r*} \alpha_2 S_{\alpha_2} & \zeta_4 Sh_{\beta_2} + k_{\eta=1}^{r*} \beta_2 Ch_{\beta_2} \\ -\zeta_2 Sh_{\beta_2} + k_{\eta=-1}^{v*} Ch_{\beta_2} & -\zeta_4 Ch_{\beta_2} - k_{\eta=-1}^{r*} \beta_2 Sh_{\beta_2} & \\ -\zeta_2 Sh_{\beta_2} + k_{\eta=1}^{v*} Ch_{\beta_2} & \zeta_4 Ch_{\beta_2} + k_{\eta=1}^{r*} \beta_2 Sh_{\beta_2} & \end{bmatrix} \begin{Bmatrix} B_1 \\ B_2 \\ B_3 \\ B_4 \end{Bmatrix} = \begin{Bmatrix} 0 \\ 0 \\ 0 \\ 0 \end{Bmatrix}, \end{aligned} \quad (45)$$

194 OR,

$$\mathbf{R}_y \mathbf{B} = \mathbf{0}, \quad (46)$$

195 where,

$$\begin{aligned} \zeta_1 &= -\alpha_2^3 - \left(\frac{4D_{66}J_3}{\alpha^2 D_{22}J_1} - \frac{D_{12}J_2}{\alpha^2 D_{22}J_1} \right) \alpha_2, \\ \zeta_2 &= \beta_2^3 - \left(\frac{4D_{66}T_3}{\alpha^2 D_{22}J_1} - \frac{D_{12}J_2}{\alpha^2 D_{22}J_1} \right) \beta_2, \\ \zeta_3 &= -\alpha_2^2 + \frac{D_{12}J_2}{\alpha^2 D_{22}J_1}, \\ \zeta_4 &= \beta_2^2 + \frac{D_{12}J_2}{\alpha^2 D_{22}J_1}. \end{aligned} \quad (47)$$

196 With the help of Equation (9b), the vertical displacement and rotation cor-
197 responding to the mode shape ψ along the y -direction at the edges $\eta = -1$
198 and $\eta = 1$ can be expressed as:

$$\begin{Bmatrix} \psi_{\eta=-1} \\ \frac{d\psi}{d\eta}_{\eta=-1} \\ \psi_{\eta=1} \\ \frac{d\psi}{d\eta}_{\eta=1} \end{Bmatrix} = \begin{bmatrix} -S_{\alpha_2} & C_{\alpha_2} & -Sh_{\beta_2} & Ch_{\beta_2} \\ \frac{\alpha_2 C_{\alpha_2}}{b} & \frac{\alpha_2 S_{\alpha_2}}{b} & \frac{\beta_2 Ch_{\beta_2}}{b} & -\frac{\beta_2 Sh_{\beta_2}}{b} \\ S_{\alpha_2} & C_{\alpha_2} & Sh_{\beta_2} & Ch_{\beta_2} \\ \frac{\alpha_2 C_{\alpha_2}}{b} & -\frac{\alpha_2 S_{\alpha_2}}{b} & \frac{\beta_2 Ch_{\beta_2}}{b} & \frac{\beta_2 Sh_{\beta_2}}{b} \end{bmatrix} \begin{Bmatrix} B_1 \\ B_2 \\ B_3 \\ B_4 \end{Bmatrix}, \quad (48)$$

199 OR,

$$\delta_y = \mathbf{Q}_y \mathbf{B}. \quad (49)$$

200 Note that the eigenvector \mathbf{B} can be expressed by multiplying the inverse
201 matrix \mathbf{Q}_y^{-1} on the left-hand side of Equation (49), and then substituting \mathbf{B}
202 into Equation (46), we obtain:

$$\mathbf{R}_y \mathbf{B} = \mathbf{R}_y \mathbf{Q}_y^{-1} \delta_y = \mathbf{0}, \quad (50)$$

203 where the dynamic stiffness matrix, denoted as $\mathbf{K}_y = \mathbf{R}_y \mathbf{Q}_y^{-1}$, can be ob-
204 tained from Equation (50).

205 3. Frequency and mode shape computation

206 3.1. Wittrick-Williams algorithm and enhancement

207 The Wittrick-Williams (W-W) algorithm [23] is an effective method for
208 determining the natural frequencies from the dynamic stiffness matrix with

209 high reliability. Instead of directly solving the equations, the algorithm com-
 210 putes the total number J of natural frequencies below a given frequency ω^* ,
 211 which is represented as:

$$J(\omega^*) = J_0(\omega^*) + s\{\mathbf{K}^\Delta(\omega^*)\} = J_0(\omega^*) + J_k(\omega^*), \quad (51)$$

212 where J_0 represents the number of natural frequencies of the structure with
 213 all ends fully clamped, \mathbf{K}^Δ is the upper triangular matrix obtained from the
 214 dynamic stiffness matrix \mathbf{K} after applying Gaussian elimination, and $J_k(\omega^*)$
 215 denotes the number of negative elements in the leading diagonal of \mathbf{K}^Δ .

216 It should be noted that the J_0 count is a crucial aspect when applying the
 217 W-W algorithm. Many previous studies use a sufficiently fine mesh or enough
 218 terms in series expansions to capture all fully clamped natural frequencies,
 219 ensuring computational accuracy [1]. However, this approach can make the
 220 application process cumbersome. To address this issue, the fully clamped
 221 problem can be replaced with a simply supported problem, where the Navier
 222 solution for the simply supported plate is used to count J_0 [18]. Nevertheless,
 223 since analytical solutions in DSM methods involve an infinite series of Fourier
 224 terms, a sufficient number of truncation terms is required to ensure accuracy
 225 and convergence.

226 In fact, J_0 can be indirectly determined by evaluating the number of
 227 natural frequencies J of the structure under specific boundary conditions,
 228 which are generally different from the original boundary conditions [8]:

$$J_0(p_1, \omega^*) = J(\bar{p}_1, \omega^*) - J_k(\bar{p}_1, \omega^*), \quad (52)$$

229 where p_1 denotes the fully clamped supports, and \bar{p}_1 denotes specific sup-
 230 ports, which are typically simply supported, guided, or a combination of the
 231 two. For these specific boundary conditions, the eigenvalue equations of SOV
 232 type solution take the form of a single harmonic function. By substituting
 233 Equation (52) into Equation (51) we get the algorithm as:

$$J(p, \omega^*) = J(\bar{p}_1, \omega^*) - J_k(\bar{p}_1, \omega^*) + J_k(p, \omega^*) \quad (53)$$

234 where p represents the original boundary conditions of the structure. There-
 235 fore, the challenge of determining $J_0(p_1, \omega^*)$ can be transformed into the
 236 problem of solving $J(\bar{p}_1, \omega^*)$ instead. By considering fully simply supported
 237 boundary conditions, the eigenvalue equation corresponding to the natural

238 frequency parameter Ω_x can be obtained from the determinant of the coeffi-
 239 cient matrix \mathbf{R}_x in Equation (25), as given by:

$$\sin 2\alpha_1 = 0. \quad (54)$$

240 With the help of Equations (21a) and (54), the closed-form solution of the
 241 n_x -th simply supported frequency Ω_{x,n_x} for the given n_y -order $\psi_{n_y}(\eta)$ can be
 242 expressed as:

$$b\Omega_{x,n_x}^4 = \left[\left(\frac{n_x\pi}{2\alpha} \right)^2 - \frac{D_{12}S_2}{D_{11}S_1} + 2\frac{D_{66}S_3}{D_{11}S_1} \right]^2 - \left(\frac{D_{12}S_2}{D_{11}S_1} - 2\frac{D_{66}S_3}{D_{11}S_1} \right)^2 + \frac{D_{22}S_4}{D_{11}S_1}. \quad (55)$$

243 For $\Omega_{x,n_x} \leq \Omega_x^* < \Omega_{x,n_x+1}$, $J(\bar{p}_1, \Omega_x^*) = n_x$. Similarly, the closed-form solution
 244 of the n_y -th simply supported frequency Ω_{y,n_y} for the given n_x -order $\phi_{n_x}(\xi)$
 245 can be expressed as:

$$a\Omega_{y,n_y}^4 = \frac{D_{22}}{D_{11}} \left\{ \left[\left(\frac{n_y\pi\alpha}{2} \right)^2 - \frac{D_{12}T_2}{D_{22}T_1} + 2\frac{D_{66}T_3}{D_{22}T_1} \right]^2 - \left(\frac{D_{12}T_2}{D_{22}T_1} - 2\frac{D_{66}T_3}{D_{22}T_1} \right)^2 + \frac{D_{11}T_4}{D_{22}T_1} \right\}. \quad (56)$$

246 For $\Omega_{y,n_y} \leq \Omega_y^* < \Omega_{y,n_y+1}$, $J(\bar{p}_1, \Omega_y^*) = n_y$. According to the relationships
 247 $\Omega_x^4 = \omega_x^2 \rho h / D_{11}$ and $\Omega_y^4 = \omega_y^2 \rho h / D_{11}$, the values of $J(\bar{p}_1, \omega_x^*)$ and $J(\bar{p}_1, \omega_y^*)$ can
 248 be derived from $J(\bar{p}_1, \Omega_x^*)$ and $J(\bar{p}_1, \Omega_y^*)$, respectively. Therefore, this refined
 249 W-W algorithm can be applied to estimate the lower and upper bounds of
 250 the frequency range, denoted as ω_l and ω_u , yielding an approximation for the
 251 frequency $\omega_a \in (\omega_l, \omega_u)$ to arbitrary precision.

252 3.2. Mode shape computation

253 The mode shape coefficients A_1 to A_4 and B_1 to B_4 in the eigenvectors \mathbf{A}
 254 and \mathbf{B} for all classic boundary conditions are provided in [27]. Alternatively,
 255 these coefficients can also be obtained through a simple numerical method,
 256 which this work presents as an approach. Here, we illustrate solving the
 257 eigenvector \mathbf{A} as an example. By assuming the exact natural frequency as
 258 ω_k , we can expand the coefficient matrix \mathbf{R}_x in Equation (25) using a first-
 259 order Taylor series about ω_a :

$$\mathbf{R}_{x,k}(\omega_k)\mathbf{A}_k = \mathbf{R}_{x,a}\mathbf{A}_k + (\omega_k - \omega_a)\mathbf{R}'_{x,a}\mathbf{A}_k + O((\omega_k - \omega_a)^2) = 0. \quad (57)$$

260 Ignoring higher-order terms, an eigenvalue problem can be derived from
 261 Equation (57):

$$(\mathbf{R}'_{x,a})^{-1} \mathbf{R}_{x,a} \mathbf{A} = (\omega_a - \omega_k) \mathbf{A} = \tau \mathbf{A}. \quad (58)$$

262 This eigenvalue problem can be solved using the inverse iteration procedure
 263 [30]:

$$\bar{\mathbf{A}}^{(i+1)} = \mathbf{R}_{x,a}^{-1} \mathbf{R}'_{x,a} \mathbf{A}^{(i)}, \quad (59)$$

264 where the initial guess for $\mathbf{A}^{(0)}$ is a column vector consisting of four randomly
 265 generated elements, each of which falls within the range (0,1). The updated
 266 eigenvalue for the next step can be obtained as:

$$\tau^{(i+1)} = \frac{1}{\bar{A}_j^{(i+1)}}, \quad (60)$$

267 where,

$$|\bar{A}_j^{(i+1)}| = \max(|\bar{A}_1^{(i+1)}|, |\bar{A}_2^{(i+1)}|, |\bar{A}_3^{(i+1)}|, |\bar{A}_4^{(i+1)}|). \quad (61)$$

268 The updated eigenvector can be obtained as:

$$\mathbf{A}^{(i+1)} = \tau^{(i+1)} \bar{\mathbf{A}}^{(i+1)}. \quad (62)$$

269 The procedure can be controlled by the error tolerance ϵ or maximum allowed
 270 steps i_{\max} :

$$\max |A_n^{(i+1)} - A_n^{(i)}| < \epsilon, \quad (63a)$$

$$i = i_{\max}. \quad (63b)$$

271 Note that the mode shape coefficients A_1 to A_4 obtained from $\mathbf{A}^{(i+1)}$ are
 272 applied for the elastically restrained boundary conditions.

273 3.3. Application procedure

274 The procedure of the proposed method is as follows:

- 275 • **Step 1** Assume initial integral parameters $I_1^{(0)}$, $I_2^{(0)}$, $I_3^{(0)}$, and $I_4^{(0)}$ in the
 276 y -direction. Using the given boundary conditions at $\xi = -1$ and $\xi = 1$,
 277 determine $\mathbf{K}_x^{(0)}$ from Equation (30). Then, apply the computational
 278 algorithms in Section 3.1 to compute the lower and upper bounds of the
 279 n_x -th non-dimensional frequency parameter, $2a\Omega_{l,x,n_x}^{(0)}$ and $2a\Omega_{u,x,n_x}^{(0)}$,
 280 and take the average $2a\Omega_{x,n_x}^{(0)} = (2a\Omega_{l,x,n_x}^{(0)} + 2a\Omega_{u,x,n_x}^{(0)})/2$ along with its
 281 corresponding mode shape $\phi_{n_x}^{(0)}$, where $n_x = 1, 2, 3, \dots$

- 282 • **Step 2** Use $\phi_{n_x}^{(0)}$ as the prescribed mode to determine $\mathbf{K}_y^{(1)}$ in Equa-
 283 tion (50), considering the boundary conditions at $\eta = -1$ and $\eta = 1$.
 284 Apply the computational algorithms to obtain the n_y -th frequency pa-
 285 rameter $2a\Omega_{y,n_y}^{(1)}$ and its corresponding mode shape $\psi_{n_y}^{(1)}$, where $n_y =$
 286 $1, 2, 3, \dots$. This completes the first iteration cycle.
- 287 • **Step 3** Use $\psi_{n_y}^{(1)}$ as the prescribed n_y -th mode shape in the y -direction to
 288 compute $\mathbf{K}_x^{(1)}$ from Equation (30), then determine the n_x -th frequency
 289 parameter $2a\Omega_{x,n_x}^{(1)}$ and its corresponding mode shape $\phi_{n_x}^{(1)}$.
- 290 • **Step 4** Use $\phi_{n_x}^{(1)}$ as the prescribed mode in the x -direction to com-
 291 pute the n_y -th frequency parameter $2a\Omega_{y,n_y}^{(2)}$ and its corresponding mode
 292 shape $\psi_{n_y}^{(2)}$, completing the second iteration cycle.
- 293 • **Step 5** Stop the iteration if $|2a\Omega_{x,n_x}^{(i)} - 2a\Omega_{x,n_x}^{(i+1)}| \leq \Delta 2a\Omega$ or $|2a\Omega_{y,n_y}^{(i)} -$
 294 $2a\Omega_{y,n_y}^{(i+1)}| \leq \Delta 2a\Omega$, where $\Delta 2a\Omega = 2a\Omega_u - 2a\Omega_l$. Here, $2a\Omega_l$ and $2a\Omega_u$
 295 are the lower and upper bounds of the frequency parameter range,
 296 within which the actual frequency parameter $2a\Omega$ lies, i.e., $2a\Omega \in$
 297 $(2a\Omega_l, 2a\Omega_u)$. The quantity $\Delta 2a\Omega$ represents the frequency param-
 298 eter interval used in the W-W algorithm.
- 299 • **Step 6** Finally, construct the (n_x, n_y) -th mode shape as $w(\xi, \eta) =$
 300 $\phi_{n_x}(\xi)\psi_{n_y}(\eta)$ using Equation (8).

301 4. Numerical Results

302 This section presents the numerical validation of the proposed method
 303 for classic boundary conditions and rotationally restrained boundary con-
 304 ditions. For all numerical calculations, the initial integral parameters are
 305 assumed as $I_1^{(0)} = 1$, $I_2^{(0)} = 1$, $I_3^{(0)} = 1$, and $I_4^{(0)} = 10$ in the y -direction,
 306 serving as the starting point of **Step 1** for any mode in all boundary con-
 307 ditions. In this section, the interval between the upper and lower bounds of
 308 the non-dimensional frequency parameter, $2a\Delta\Omega$, is set to 0.005, although
 309 any desired level of precision can be used. According to our numerical calcu-
 310 lations, two iteration cycles are generally sufficient to meet the convergence
 311 requirement (i.e., $|2a\Omega_x^{(i)} - 2a\Omega_x^{(i+1)}| \leq \Delta 2a\Omega$ or $|2a\Omega_y^{(i)} - 2a\Omega_y^{(i+1)}| \leq \Delta 2a\Omega$)
 312 for most cases, with at most three cycles required when applying the iterative
 313 procedure in Section 3.3.

314 4.1. Classical boundary conditions

315 In this subsection, the proposed method is validated by comparison with
 316 the extended SOV method [27]. The properties of the orthotropic plate,
 317 consistent with those in [27], are as follows: $E_1 = 185$ GPa, $E_2 = 10.5$ GPa,
 318 $G_{12} = 7.3$ GPa, $\rho = 1600$ kg m⁻¹, and $\nu_{12} = 0.28$.

319 The translational springs (k_ξ^v) and rotational springs (k_ξ^r) along all edges
 320 can be set to zero or infinity (represented as 1×10^{15} N m⁻¹ in the numerical
 321 calculations of this study) to obtain different classic boundary conditions.

322 The results for SSSS, SCSF, GCGC, CCCC, SSCC, SCCC, GGCC, CCFF,
 323 CFCC, CFFF, and FFFF boundary conditions are presented in Tables 1 to 3.
 324 Note that, as is convention, S is a simple support (rotation, no translation),
 325 C is a clamped supported (no rotation or translation), G is a guided support
 326 (translation, no rotation), and F is a free edge. These results demonstrate
 327 high accuracy compared to the extended SOV method, with difference re-
 328 maining smaller than the frequency parameter interval $2a\Delta\Omega = 0.005$. The
 329 frequency parameters in both directions are equal ($2a\Omega_x - 2a\Omega_y = 0$) in al-
 330 most all cases, with a few exceptions where $2a\Omega_x - 2a\Omega_y = 0.005$. In fact,
 331 higher accuracy compared to the extended SOV method can be achieved if
 332 the frequency parameter interval $2a\Delta\Omega$ is set smaller than 0.005. It should be
 333 noted that the accuracy improves only by reducing $2a\Delta\Omega$, and no additional
 334 iterations are required according to our calculations. Figure 2 shows the first
 335 six nonzero mode shapes of a square orthotropic plate with FFFF bound-
 336 ary conditions, where the mode shape coefficients are calculated using the
 337 numerical method developed in this study. Instead of selecting fixed expres-
 338 sions for the mode shape coefficients based on specific boundary conditions,
 339 our method is applicable to all boundary conditions.

340 4.2. Rotational spring-supported edges

341 In this subsection, rectangular orthotropic plates with rotational spring-
 342 supported edges with no translations ($k_\xi^v = k_\eta^v = \infty$) are examined. The
 343 rotational stiffness coefficients are defined as:

$$r_\xi = \frac{2ak_\xi^r}{D_{11}}, \quad (64a)$$

$$r_\eta = \frac{2bk_\eta^r}{D_{22}}. \quad (64b)$$

344 The first example considers a square isotropic plate with all four edges ro-
 345 tationally restrained. The vertical translational springs along the four edges

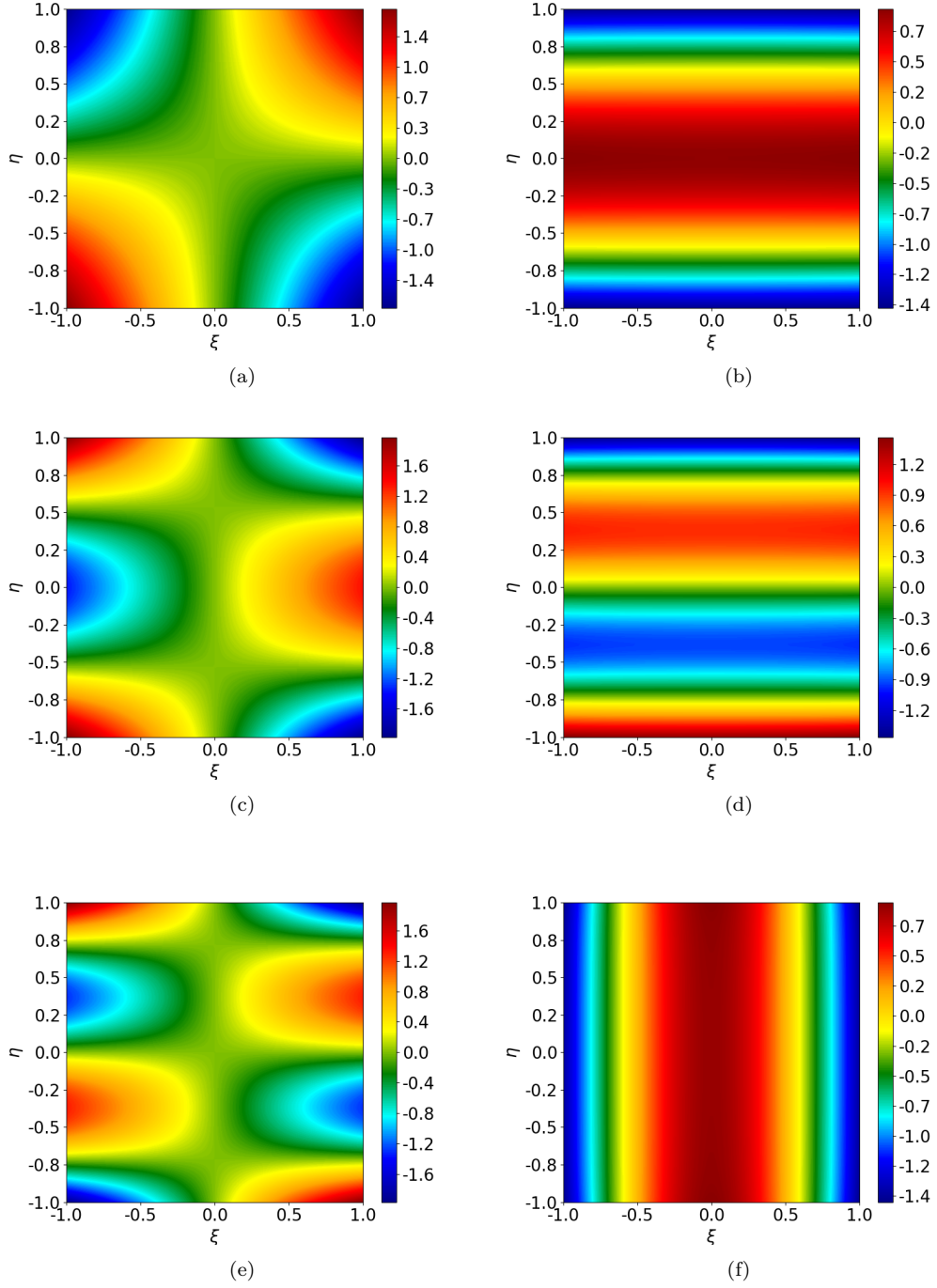


Figure 2: The first six nonzero mode shapes of a square orthotropic plate with FFFF boundary conditions: (a) the first mode; (b) the second mode; (c) the third mode; (d) the fourth mode; (e) the fifth mode; (f) the sixth mode.

Table 1: The first seven frequency parameter $2a\Omega$ of of orthotropic rectangular plates with SSSS, SCSF and GCGC boundary conditions.

BCs	α	Mode	$2a\Omega_x = 2a\Omega_y = 2a\sqrt{\rho h\omega^2/D_{11}}$						
			1	2	3	4	5	6	7
SSSS	0.5	Mode number	(1,1)	(1,2)	(1,3)	(1,4)	(1,5)	(1,6)	(1,7)
		extended SOV 27	3.1807	3.3190	3.5938	4.0135	4.5495	5.1635	5.8265
		Present	3.1825	3.3225	3.5975	4.0175	4.5525	5.1625	5.8275
	1	Mode number	(1,1)	(1,2)	(1,3)	(2,1)	(1,4)	(2,2)	(2,3)
		extended SOV 27	3.3190	4.0135	5.1635	6.3615	6.5200	6.6379	7.1876
		Present	3.3175	4.0175	5.1625	6.3625	6.5175	6.6375	7.1875
	1.5	Mode number	(1,1)	(1,2)	(2,1)	(2,2)	(1,3)	(2,3)	(1,4)
		extended SOV 27	3.5938	5.1635	6.4698	7.1876	7.2331	8.5389	9.4352
		Present	3.5975	5.1675	6.4725	7.1875	7.2325	8.5375	9.4375
SCSF	0.5	Mode number	(1,1)	(1,2)	(1,3)	(1,4)	(1,5)	(1,6)	(1,7)
		extended SOV 27	3.1516	3.2451	3.4588	3.8131	4.2950	4.8711	5.5087
		Present	3.1525	3.2475	3.4575	3.8175	4.2925	4.8725	5.5075
	1	Mode number	(1,1)	(1,2)	(1,3)	(1,4)	(2,1)	(2,2)	(2,3)
		extended SOV 27	3.1908	3.6428	4.5972	5.8599	6.3033	6.4901	6.9177
		Present	3.1925	3.6425	4.5975	5.8575	6.3025	6.4925	6.9175
	1.5	Mode number	(1,1)	(1,2)	(1,3)	(2,1)	(2,2)	(2,3)	(1,4)
		extended SOV 27	3.2710	4.3430	6.2157	6.3337	6.8043	7.8718	8.3518
		Present	3.2725	4.3425	6.2175	6.3325	6.8025	7.8725	8.3525
GCGC	0.5	Mode number	(1,1)	(1,2)	(1,3)	(2,1)	(2,2)	(1,4)	(2,3)
		extended SOV 27	1.1544	1.9166	2.6835	3.1983	3.3890	3.4501	3.7372
		Present	1.1525	1.9175	2.6825	3.1975	3.3875	3.4525	3.7375
	1	Mode number	(1,1)	(2,1)	(1,2)	(2,2)	(1,3)	(2,3)	(3,1)
		extended SOV 27	2.3087	3.4900	3.8331	4.4682	5.3669	5.7736	6.3967
		Present	2.3075	3.4875	3.8325	4.4675	5.3675	5.7725	6.3975
	1.5	Mode number	(1,1)	(2,1)	(1,2)	(2,2)	(3,1)	(3,2)	(1,3)
		extended SOV 27	3.4631	4.1353	5.7497	6.0981	6.6049	7.6449	8.0504
		Present	3.4625	4.1325	5.7475	6.0975	6.6075	7.6425	8.0525

Table 2: The first seven frequency parameter $2a\Omega$ of of orthotropic rectangular plates with CCCC, SSCC, SCCC and GGCC boundary conditions.

BCs	α	Mode	$2a\Omega_x = 2a\Omega_y = 2a\sqrt{\rho h \omega^2 / D_{11}}$						
			1	2	3	4	5	6	7
CCCC	0.5	Mode number	(1,1)	(1,2)	(1,3)	(1,4)	(1,5)	(1,6)	(1,7)
		extended SOV 27	4.7500	4.8208	4.9682	5.2177	5.5791	6.0430	6.5892
		Present	4.7475	4.8225	4.9725	5.2175	5.5825	6.0425	6.5875
	1	Mode number	(1,1)	(1,2)	(1,3)	(1,4)	(2,1)	(2,2)	(2,3)
		extended SOV 27	4.8579	5.3546	6.2819	7.4972	7.9193	8.1490	8.6054
		Present	4.8575	5.3575	6.2875	7.4975	7.9175	8.1475	8.6075
	1.5	Mode number	(1,1)	(1,2)	(2,1)	(1,3)	(2,2)	(2,3)	(1,4)
		extended SOV 27	5.1581	6.5412	8.0409	8.4945	8.7204	9.9793	10.6460
		Present	5.1575	6.5375	8.0425	8.4975	8.7175	9.9775	10.6425
SSCC	0.5	Mode number	(1,1)	(1,2)	(1,3)	(1,4)	(1,5)	(1,6)	(1,7)
		extended SOV 27	3.9542	4.0520	4.2525	4.5785	5.0254	5.5682	6.1789
		Present	3.9575	4.0525	4.2475	4.5775	5.0225	5.5725	6.1825
	1	Mode number	(1,1)	(1,2)	(1,3)	(1,4)	(2,1)	(2,2)	(2,3)
		extended SOV 27	4.0745	4.6606	5.7009	6.9940	7.1396	7.3894	7.8881
		Present	4.0775	4.6625	5.7025	6.9925	7.1375	7.3875	7.8875
	1.5	Mode number	(1,1)	(1,2)	(2,1)	(1,3)	(2,2)	(2,3)	(1,4)
		extended SOV 27	4.3602	5.8384	7.2531	7.8560	7.9481	9.2515	10.0366
		Present	4.3625	5.8325	7.2525	7.8575	7.9525	9.2525	10.0325
SCCC	0.5	Mode number	(1,1)	(1,2)	(1,3)	(1,4)	(1,5)	(1,6)	(1,7)
		extended SOV 27	3.9596	4.0745	4.3027	4.6606	5.1361	5.7009	6.3271
		Present	3.9575	4.0725	4.3025	4.6625	5.1325	5.7025	6.3325
	1	Mode number	(1,1)	(1,2)	(1,3)	(2,1)	(1,4)	(2,2)	(2,3)
		extended SOV 27	4.1349	4.8478	5.9805	7.1541	7.3192	7.4478	8.0121
		Present	4.1325	4.8475	5.9825	7.1525	7.3175	7.4475	8.0125
	1.5	Mode number	(1,1)	(1,2)	(2,1)	(2,2)	(1,3)	(2,3)	(3,1)
		extended SOV 27	4.5824	6.2766	7.3116	8.1528	8.3705	9.5986	10.3507
		Present	4.5825	6.2775	7.3125	8.1525	8.3725	9.5975	10.3525
GGCC	0.5	Mode number	(1,1)	(1,2)	(1,3)	(1,4)	(1,5)	(1,6)	(1,7)
		extended SOV 27	2.3750	2.4841	2.7895	3.2946	3.9226	4.6123	5.3326
		Present	2.3725	2.4875	2.7925	3.2975	3.9225	4.6075	5.3325
	1	Mode number	(1,1)	(1,2)	(1,3)	(2,1)	(2,2)	(1,4)	(2,3)
		extended SOV 27	2.4290	3.1410	4.4293	5.5202	5.7315	5.8801	6.2606
		Present	2.4325	3.1425	4.4325	5.5225	5.7325	5.8775	6.2625
	1.5	Mode number	(1,1)	(1,2)	(2,1)	(2,2)	(1,3)	(2,3)	(3,1)
		extended SOV 27	2.5790	4.2472	5.5565	6.1533	6.4347	7.5231	8.6732
		Present	2.5825	4.2475	5.5575	6.1525	6.4325	7.5225	8.6725

Table 3: The first seven nonzero frequency parameter $2a\Omega$ of of orthotropic rectangular plates with CCFF, CFCF, CFFF and FFFF boundary conditions.

BCs	α	Mode	$2a\Omega_x = 2a\Omega_y = 2a\sqrt{\rho h \omega^2 / D_{11}}$						
			1	2	3	4	5	6	7
CCFF	0.5	Mode number	(1,1)	(1,2)	(1,3)	(1,4)	(1,5)	(1,6)	(2,1)
		extended SOV 27	1.8978	2.0905	2.4925	3.0563	3.7110	4.4117	4.7029
		Present	1.8975	2.0925	2.4925	3.0575	3.7125	4.4125	4.7025
	1	Mode number	(1,1)	(1,2)	(1,3)	(2,1)	(2,2)	(1,4)	(2,3)
		extended SOV 27	1.9930	2.7895	4.0733	4.7338	5.0652	5.5128	5.7419
		Present	1.9925	2.7875	4.0725	4.7325	5.0675	5.5125	5.7425
	1.5	Mode number	(1,1)	(1,2)	(2,1)	(2,2)	(1,3)	(2,3)	(3,1)
		extended SOV 27	2.1780	3.7411	4.7931	5.5758	5.8895	7.0263	7.9006
		Present	2.1775	3.7425	4.7925	5.5725	5.8875	7.0275	7.9025
CFCF	0.5	Mode number	(1,1)	(1,2)	(1,3)	(1,4)	(1,5)	(1,6)	(1,7)
		extended SOV 27	4.7297	4.7427	4.7881	4.8819	5.0478	5.3072	5.6694
		Present	4.7275	4.7425	4.7875	4.8825	5.0475	5.3075	5.6675
	1	Mode number	(1,1)	(1,2)	(1,3)	(1,4)	(1,5)	(1,6)	(2,1)
		extended SOV 27	4.7295	4.7817	5.0012	5.5348	6.4407	7.6182	7.8523
		Present	4.7275	4.7825	5.0025	5.5325	6.4425	7.6175	7.8525
	1.5	Mode number	(1,1)	(1,2)	(1,3)	(1,4)	(2,1)	(2,2)	(2,3)
		extended SOV 27	4.7292	4.8458	5.4221	6.7635	7.8518	7.9470	8.3021
		Present	4.7275	4.8475	5.4225	6.7625	7.8525	7.9475	8.3025
CFFF	0.5	Mode number	(1,1)	(1,2)	(1,3)	(1,4)	(1,5)	(1,6)	(1,7)
		extended SOV 27	1.8751	1.9439	2.1679	2.5657	3.1106	3.7486	4.4382
		Present	1.8775	1.9425	2.1675	2.5675	3.1125	3.7475	4.4375
	1	Mode number	(1,1)	(1,2)	(1,3)	(1,4)	(2,1)	(2,2)	(2,3)
		extended SOV 27	1.8750	2.1242	2.9077	4.1319	4.6937	4.8226	5.2263
		Present	1.8775	2.1225	2.9075	4.1325	4.6925	4.8225	5.2275
	1.5	Mode number	(1,1)	(1,2)	(1,3)	(2,1)	(2,2)	(2,3)	(1,4)
		extended SOV 27	1.8750	2.3402	3.8522	4.6935	4.9753	5.8314	5.9292
		Present	1.8775	2.3425	3.8525	4.6925	4.9775	5.8325	5.9275
FFFF	0.5	Mode number	(1,3)	(2,2)	(1,4)	(2,3)	(1,5)	(2,4)	(2,5)
		extended SOV 27	1.1540	1.4858	1.9157	2.1704	2.6821	2.7881	3.4093
		Present	1.1525	1.4875	1.9175	2.1725	2.6825	2.7875	3.4075
	1	Mode number	(2,2)	(1,3)	(2,3)	(1,4)	(2,4)	(3,1)	(3,2)
		extended SOV 27	2.1311	2.3082	3.2734	3.8320	4.4962	4.7298	4.9138
		Present	2.1325	2.3075	3.2725	3.8325	4.4975	4.7275	4.9125
	1.5	Mode number	(2,2)	(1,3)	(2,3)	(3,1)	(3,2)	(1,4)	(3,3)
		extended SOV 27	2.6277	3.4625	4.2915	4.7296	5.1259	5.7485	6.1588
		Present	2.6275	3.4625	4.2925	4.7275	5.1275	5.7475	6.1575

are numerically set as $k_{\xi=-1}^v = k_{\xi=1}^v = k_{\eta=-1}^v = k_{\eta=1}^v = 1 \times 10^{12} \text{ N m}^{-1}$. The material properties are given as $D_{11} = D_{22} = D_3$ and $\nu_{12} = \nu_{21} = 0.3$.

Table 4 presents the frequency parameter $2a\Omega$ for different rotational stiffness coefficients $r_\xi = r_\eta$ with values 0.1, 1, 10, 100, and 1000. Notably, when $r_\xi = r_\eta = 0$ and $r_\xi = r_\eta = \infty$, the boundary conditions correspond to SSSS and CCCC, respectively.

Interestingly, the results indicate that the frequencies Ω_x and Ω_y are not strictly equal for some mode shapes under these boundary conditions. The actual frequency Ω lies between Ω_x and Ω_y , which may be attributed to the fact that Ω_x and Ω_y satisfy Rayleigh's principle in Equation (3), representing the weak-form governing equations, but do not necessarily satisfy the strong-form governing equations in Equation (1). For a physical problem with exact solutions, both Equations (1) and (3) must be satisfied. If this condition is not met, applying Equation (3) still provides a viable approach for approximating the exact solution of the plate. Thus, the exact frequency can be estimated as $\Omega = (\Omega_x + \Omega_y)/2$. As shown in Table 4, the maximum difference between Ω and the solutions reported in 31 is less than 1.3%. Figure 3 illustrates the variation in mode shapes corresponding to the fundamental natural frequency as the rotational stiffness $r_\xi = r_\eta$ increases from zero to ∞ , transitioning the boundary conditions from SSSS to CCCC.

The next example considers a rectangular orthotropic plate with three simply supported edges ($k_{\xi=-1}^r = k_{\xi=1}^r = k_{\eta=1}^r = 0$), while the edge at $\eta = -1$ is rotationally restrained. The material properties are consistent with those in 31, where $2D_{11} = 2D_{22} = D_3$ and $\nu_{12} = \nu_{21} = 0.3$. Table 5 shows the fundamental frequency results for different length ratios (b/a), comparing them with those reported in 31. The maximum observed difference is 0.8% when $r_{\eta=-1} = 10$.

Interestingly, in certain numerical calculations involving rotationally restrained boundary conditions, the variables α_1 and α_2 may take complex values rather than being purely real. Consequently, the mode shape coefficients A_1 , A_2 , B_1 , and B_2 become complex-valued, leading to \mathbf{R} and \mathbf{Q}^{-1} being complex matrices. However, the mode shapes $\phi(\xi)$ and $\psi(\eta)$ remain real-valued, and the dynamic stiffness matrix $\mathbf{K} = \mathbf{R}\mathbf{Q}^{-1}$ is a real symmetric matrix. Thus, the frequency Ω can be obtained by solving \mathbf{K} using the refined W-W algorithm provided in this study, which avoids solving the eigenvalue equations in both the real and complex domains.

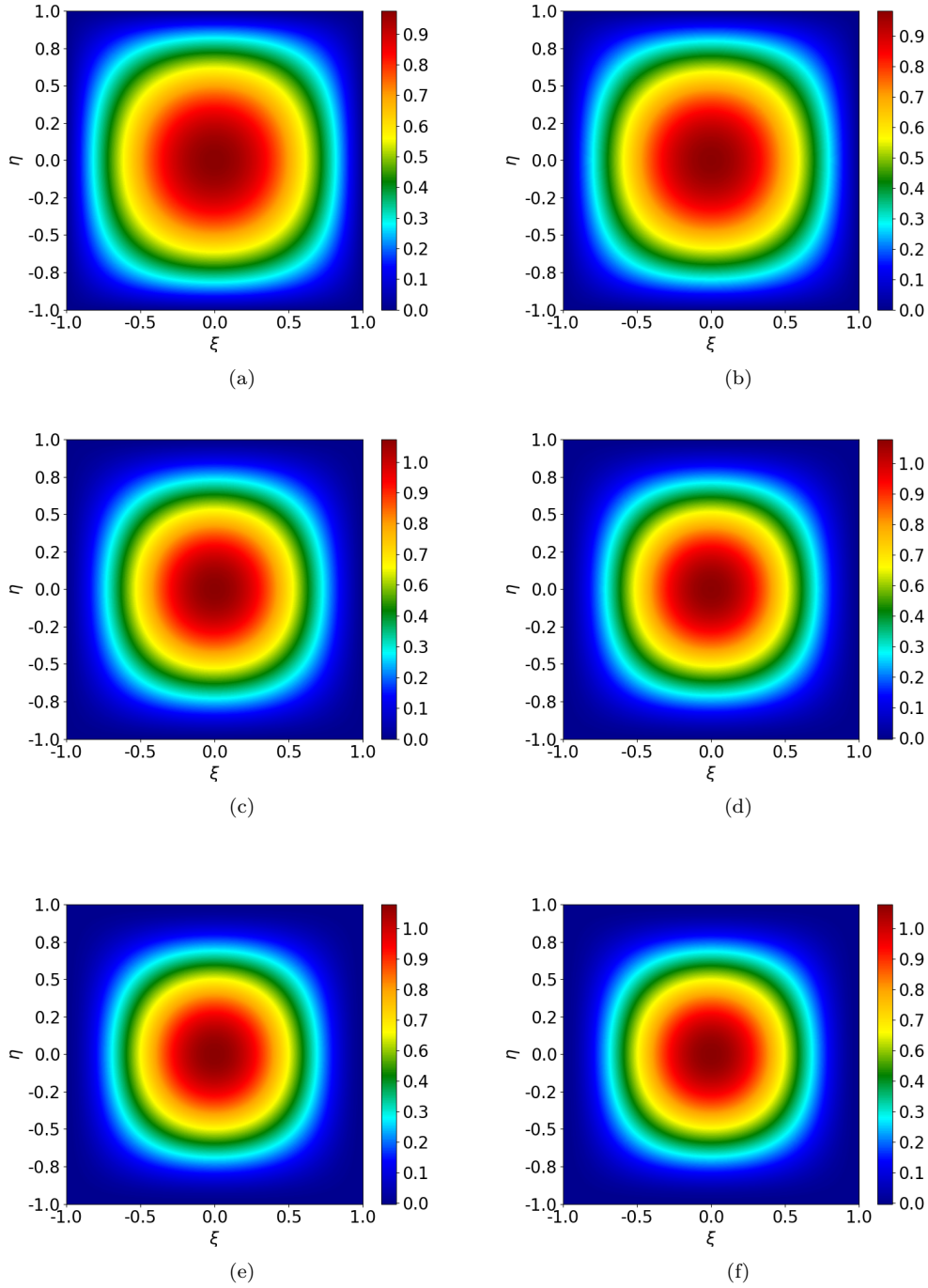


Figure 3: The first mode shape of a square isotropic plate with all four edges rotationally restrained: (a) $r_\xi = r_\eta = 0$; (b) $r_\xi = r_\eta = 1$; (c) $r_\xi = r_\eta = 10$; (d) $r_\xi = r_\eta = 20$; (e) $r_\xi = r_\eta = 100$; (f) $r_\xi = r_\eta = \infty$.

Table 4: The first six frequency parameters, $2a\Omega = 2a\sqrt[4]{\rho h\omega^2/D_{11}}$, of a square isotropic plate with all four edges rotationally restrained, where $k_{\xi=-1}^r = k_{\xi=1}^r = k_{\eta=-1}^r = k_{\eta=1}^r$.

r	Mode	$2a\Omega$					
		1	2	3	4	5	6
0.1	Mode number	(1,1)	(1,2)	(2,1)	(2,2)	(1,3)	(3,1)
	Ref.20	4.454	6.992	7.045	8.890	9.782	9.960
	Ref.31	4.465	7.039	7.039	8.897	9.945	9.945
	Present (Ω_x)	4.463	7.028	7.043	8.893	9.938	9.953
	Present (Ω_y)	4.463	7.043	7.028	8.893	9.953	9.938
	Present (Ω)	4.463	7.035	7.035	8.893	9.945	9.945
	Difference (%)	0.044	0.056	0.056	0.044	0.000	0.000
1	Mode number	(1,1)	(1,2)	(2,1)	(2,2)	(3,1)	(1,3)
	Ref.20	4.529	7.008	7.136	8.936	9.787	10.036
	Ref.31	4.637	7.155	7.155	8.991	10.029	10.030
	Present (Ω_x)	4.648	7.098	7.223	8.993	10.093	9.968
	Present (Ω_y)	4.648	7.223	7.098	8.993	9.968	10.098
	Present (Ω)	4.648	7.160	7.160	8.993	10.030	10.033
	Difference (%)	0.237	0.069	0.069	0.022	0.009	0.029
10	Mode number	(1,1)	(1,2)	(2,1)	(2,2)	(1,3)	(3,1)
	Ref.31	5.346	7.768	7.768	9.537	10.552	10.563
	Present (Ω_x)	5.413	7.718	7.953	9.598	10.448	10.782
	Present (Ω_y)	5.413	7.953	7.718	9.598	10.782	10.453
	Present (Ω)	5.413	7.835	7.835	9.598	10.615	10.618
	Difference (%)	1.253	0.862	0.862	0.639	0.597	0.520
100	Mode number	(1,1)	(1,2)	(2,1)	(2,2)	(1,3)	(3,1)
	Ref.20	5.895	8.326	8.422	10.167	10.957	11.297
	Ref.31	5.901	8.442	8.442	10.253	11.307	11.333
	Present (Ω_x)	5.913	8.428	8.473	10.258	11.293	11.373
	Present (Ω_y)	5.913	8.473	8.478	10.258	11.373	11.293
	Present (Ω)	5.913	8.450	8.450	10.258	11.333	11.333
	Difference (%)	0.203	0.094	0.094	0.048	0.229	0.000
1000	Mode number	(1,1)	(1,2)	(2,1)	(2,2)	(1,3)	(3,1)
	Ref.31	6.011	8.585	8.585	10.424	11.495	11.522
	Present (Ω_x)	5.988	8.553	8.553	10.388	11.463	11.478
	Present (Ω_y)	5.988	8.553	8.553	10.388	11.478	11.463
	Present (Ω)	5.988	8.553	8.553	10.388	11.470	11.470
	Difference (%)	0.382	0.372	0.372	0.345	0.217	0.451

Table 5: Fundamental frequency parameter $2a\Omega = 2a\sqrt[4]{\rho h\omega^2/D_{11}}$ of rectangular orthotropic plates with three edges simply supported ($k_{\xi=-1}^r = k_{\xi=1}^r = k_{\eta=1}^r = 0$) and the edge at $\eta = -1$ rotationally restrained.

b/a	$r_{\eta=-1}$	$2a\Omega$				
		Ref.31	Present (Ω)	Present (Ω_x)	Present (Ω_y)	Difference (%)
0.5	0	7.530	7.523	7.523	7.523	0.092
	1	7.690	7.700	7.588	7.813	0.130
	10	8.250	8.308	8.198	8.418	0.703
	∞	8.705	8.695	8.695	8.695	0.114
1.0	0	4.917	4.918	4.918	4.918	0.020
	1	4.954	4.960	4.933	4.988	0.121
	10	5.114	5.128	5.088	5.168	0.273
	∞	5.289	5.278	5.278	5.278	0.207
1.5	0	4.126	4.128	4.128	4.128	0.048
	1	4.139	4.138	4.128	4.148	0.024
	10	4.202	4.208	4.188	4.228	0.142
	∞	4.292	4.288	4.288	4.288	0.093

382 5. Conclusion

383 In this study, the dynamic stiffness matrix (DSM) based on the ex-
384 tended separation-of-variable (SOV) solution has been developed for the
385 vibration analysis of an orthotropic rectangular plate with general homo-
386 geneous boundary conditions.

387 Instead of solving highly nonlinear eigenvalue equations involved in the
388 SOV methods, the extended SOV solution is adopted to construct the dy-
389 namic stiffness matrices. Several novel techniques have proposed to solve
390 the eigenvalue problem and mode shape computation. The challenge of de-
391 termining the fully clamped frequencies using the Wittrick-Williams (W-W)
392 algorithm is resolved by computing the frequencies under specific boundary
393 conditions, whose closed-form expression can be easily derived using the SOV
394 method.

395 Classical boundary conditions, such as guided, simply supported, clamped,
396 and free edges, can be realized by setting the translational springs (k_ξ^v) and
397 rotational springs (k_ξ^r) along the plate edges to either zero or infinity, as
398 appropriate. Numerical experiments validate the accuracy of this approach
399 for these boundary conditions. The results shows that the SOV solution can
400 also be extended to handle elastically-restrained boundary conditions. De-
401 spite certain approximations inherent in some elastically-restrained cases, the
402 maximum percentage error across all numerical experiments remains within
403 1.25%. This may occur because the SOV solution used is derived from the
404 weak-form governing equation, which is based on Rayleigh's principle.

405 Since the SOV solution $\phi(\xi)\psi(\eta)$ consists of only a single term for each
406 mode order, unlike the infinite series expansions used in the traditional DSM,
407 each eigenvalue solution can be explicitly expressed. This suggests the po-
408 tential for obtaining more concise solutions for assembled plate structures
409 compared to traditional DSM methods.

410 Finally, the developments reported in this paper should find good ap-
411 plication with researchers and practitioners interested in the vibration of
412 generally-supported rectangular orthotropic plates.

413 Appendix A Integral parameters

414 The integral parameters I_1 , I_2 , I_3 , and I_4 are defined as follows:

$$\begin{aligned}
 I_1 &= \int_0^1 \psi^2 d\eta \\
 &= (B_1^2 + B_2^2 - B_3^2 + B_4^2) + \frac{-B_1^2 + B_2^2}{2\alpha_2} \sin(2\alpha_2) + \frac{B_3^2 + B_4^2}{2\beta_2} \sinh(2\beta_2) \\
 &\quad + \frac{4(\alpha_2 B_2 B_4 + \beta_2 B_1 B_3)}{\alpha_2^2 + \beta_2^2} \sin(\alpha_2) \cosh(\beta_2) \\
 &\quad + \frac{4(-\alpha_2 B_1 B_3 + \beta_2 B_2 B_4)}{\alpha_2^2 + \beta_2^2} \cos(\alpha_2) \sinh(\beta_2).
 \end{aligned}
 \tag{A.1}$$

$$\begin{aligned}
 I_2 &= \int_0^1 \left(\psi \frac{d^2 \psi}{d\eta^2} \right) d\eta \\
 &= \left(-\alpha_2^2 B_1^2 - \alpha_2^2 B_2^2 - \beta_2^2 B_3^2 + \beta_2^2 B_4^2 \right) \\
 &\quad + \frac{\alpha_2(B_1^2 - B_2^2)}{2} \sin(2\alpha_2) + \frac{\beta_2(B_3^2 + B_4^2)}{2} \sinh(2\beta_2) \\
 &\quad + \frac{2(-\alpha_2^2 + \beta_2^2)(\alpha_2 B_2 B_4 + \beta_2 B_1 B_3)}{\alpha_2^2 + \beta_2^2} \sin(\alpha_2) \cosh(\beta_2) \\
 &\quad + \frac{2(-\alpha_2^2 + \beta_2^2)(-\alpha_2 B_1 B_3 + \beta_2 B_2 B_4)}{\alpha_2^2 + \beta_2^2} \cos(\alpha_2) \sinh(\beta_2).
 \end{aligned}
 \tag{A.2}$$

$$\begin{aligned}
 I_3 &= \int_0^1 \left(\frac{d\psi}{d\eta} \right)^2 d\eta \\
 &= \alpha_2^2 B_1^2 + \alpha_2^2 B_2^2 + \beta_2^2 B_3^2 - \beta_2^2 B_4^2 \\
 &\quad + \frac{\alpha_2(B_1^2 - B_2^2)}{2} \sin(2\alpha_2) + \frac{\beta_2(B_3^2 + B_4^2)}{2} \sinh(2\beta_2) \\
 &\quad + \frac{4\alpha_2\beta_2(\alpha_2 B_1 B_3 - \beta_2 B_2 B_4)}{\alpha_2^2 + \beta_2^2} \sin(\alpha_2) \cosh(\beta_2) \\
 &\quad + \frac{4\alpha_2\beta_2(\alpha_2 B_2 B_4 + \beta_2 B_1 B_3)}{\alpha_2^2 + \beta_2^2} \cos(\alpha_2) \sinh(\beta_2).
 \end{aligned}
 \tag{A.3}$$

$$\begin{aligned}
I_4 &= \int_0^1 \left(\frac{d^2 \psi}{d\eta^2} \right)^2 d\eta \\
&= \left(\alpha_2^4 B_1^2 + \alpha_2^4 B_2^2 - \beta_2^4 B_3^2 + \beta_2^4 B_4^2 \right) \\
&\quad + \frac{\alpha_2^3 (-B_1^2 + B_2^2)}{2} \sin(2\alpha_2) + \frac{\beta_2^3 (B_3^2 + B_4^2)}{2} \sinh(2\beta_2) \\
&\quad + \frac{4\alpha_2^2 \beta_2^2 (-\alpha_2 B_2 B_4 - \beta_2 B_1 B_3)}{\alpha_2^2 + \beta_2^2} \sin(\alpha_2) \cosh(\beta_2) \\
&\quad + \frac{4\alpha_2^2 \beta_2^2 (\alpha_2 B_1 B_3 - \beta_2 B_2 B_4)}{\alpha_2^2 + \beta_2^2} \cos(\alpha_2) \sinh(\beta_2)
\end{aligned} \tag{A.4}$$

418 The integral parameters J_1 , J_2 , J_3 , and J_4 can be obtained by replacing B_1
419 to B_4 by A_1 to A_4 , respectively, and α_2 and β_2 by α_1 and β_1 , respectively.

420 References

- 421 [1] Banerjee, J., Papkov, S., Liu, X., Kennedy, D., 2015. Dynamic stiffness
422 matrix of a rectangular plate for the general case. *Journal of Sound and*
423 *Vibration* 342, 177–199. doi:10.1016/j.jsv.2014.12.031.
- 424 [2] Banerjee, J.R., 1997. Dynamic stiffness formulation for structural el-
425 ements: a general approach. *Computers & Structures* 63, 101–103.
426 doi:10.1016/S0045-7949(96)00326-4.
- 427 [3] Biancolini, M.E., Brutti, C., Reccia, L., 2005. Approximate solution for
428 free vibrations of thin orthotropic rectangular plates. *Journal of Sound*
429 *and Vibration* 288, 321–344. doi:10.1016/j.jsv.2005.01.005.
- 430 [4] Boscolo, M., Banerjee, J., 2011. Dynamic stiffness elements and their ap-
431 plications for plates using first order shear deformation theory. *Comput-*
432 *ers & Structures* 89, 395–410. doi:10.1016/j.compstruc.2010.11.005.
- 433 [5] Fazzolari, F., Boscolo, M., Banerjee, J., 2013. An exact dynamic stiffness
434 element using a higher order shear deformation theory for free vibration
435 analysis of composite plate assemblies. *Composite Structures* 96, 262–
436 278. doi:10.1016/j.compstruct.2012.08.033.
- 437 [6] Ghorbel, O., Casimir, J.B., Hammami, L., Tawfiq, I., Haddar, M., 2015.
438 Dynamic stiffness formulation for free orthotropic plates. *Journal of*
439 *Sound and Vibration* 346, 361–375. doi:10.1016/j.jsv.2015.02.020.

- 440 [7] Gorman, D.J., 2005. Free in-plane vibration analysis of rectangular
441 plates with elastic support normal to the boundaries. *Journal of Sound*
442 *and Vibration* 285, 941–966. doi:10.1016/j.jsv.2004.09.017.
- 443 [8] Han, F., Dan, D., Cheng, W., Zang, J., 2018. An improved wittrick-
444 williams algorithm for beam-type structures. *Composite Structures* 204,
445 560–566. doi:10.1016/j.compstruct.2018.07.108.
- 446 [9] Kantorovich, L.V., Krylov, V.I., 1958. *Approximate Methods of Higher*
447 *Analysis*. Interscience Publishers, New York.
- 448 [10] Kerr, A.D., 1968. An extension of the kantorovich method. *Quarterly*
449 *of Applied Mathematics* 26, 219–229. doi:10.1090/qam/99857.
- 450 [11] Khov, H., Li, W.L., Gibson, R.F., 2009. An accurate solution method
451 for the static and dynamic deflections of orthotropic plates with general
452 boundary conditions. *Composite Structures* 90, 474–481. doi:10.1016/
453 j.compstruct.2009.04.020.
- 454 [12] Laura, P.A., Saffell Jr, B.F., 1967. Study of small-amplitude vibrations
455 of clamped rectangular plates using polynomial approximations. *The*
456 *Journal of the Acoustical Society of America* 41, 836–839. doi:10.1121/
457 1.1910414.
- 458 [13] Leissa, A.W., 1973. The free vibration of rectangular plates. *Jour-*
459 *nal of Sound and Vibration* 31, 257–293. doi:10.1016/S0022-460X(73)
460 80371-2.
- 461 [14] Levy, M., 1899. Sur l’équilibre élastique d’une plaque rectangulaire.
462 *Comptes Rendus Acad. Sci. Paris* 129, 535–539.
- 463 [15] Li, R., Zhong, Y., Tian, B., Liu, Y., 2009a. On the finite integral trans-
464 form method for exact bending solutions of fully clamped orthotropic
465 rectangular thin plates. *Applied Mathematics Letters* 22, 1821–1827.
466 doi:10.1016/j.aml.2009.07.003.
- 467 [16] Li, W.L., 2004. Vibration analysis of rectangular plates with general
468 elastic boundary supports. *Journal of Sound and Vibration* 273, 619–
469 635. doi:10.1016/S0022-460X(03)00562-5.

- [17] Li, W.L., Zhang, X., Du, J., Liu, Z., 2009b. An exact series solution for the transverse vibration of rectangular plates with general elastic boundary supports. *Journal of Sound and Vibration* 321, 254–269. doi:10.1016/j.jsv.2008.09.035.
- [18] Liu, X., Banerjee, J., 2015. An exact spectral-dynamic stiffness method for free flexural vibration analysis of orthotropic composite plate assemblies—part i: Theory. *Composite Structures* 132, 1274–1287. doi:10.1016/j.compstruct.2015.07.020.
- [19] Liu, X., Banerjee, J., 2016. Free vibration analysis for plates with arbitrary boundary conditions using a novel spectral-dynamic stiffness method. *Computers & Structures* 164, 108–126. doi:10.1016/j.compstruc.2015.11.005.
- [20] Mukhopadhyay, M., 1979. Free vibration of rectangular plates with edges having different degrees of rotational restraint. *Journal of Sound and Vibration* 67, 459–468.
- [21] Navier, L., 1823. Extrait des recherches sur la flexion des plans elastiques. *Bull. Sci. Soc. Philomat.* , 95–102.
- [22] Timoshenko, S., 1940. *Theory of Plates and Shells*. McGraw-Hill Book Company.
- [23] Wittrick, W.H., Williams, F.W., 1971. A general algorithm for computing natural frequencies of elastic structures. *The Quarterly Journal of Mechanics and Applied Mathematics* 24, 263–284. doi:10.1093/qjmam/24.3.263.
- [24] Xing, Y., Li, G., Yuan, Y., 2022. A review of the analytical solution methods for the eigenvalue problems of rectangular plates. *International Journal of Mechanical Sciences* 221, 107171. doi:10.1016/j.ijmecsci.2022.107171.
- [25] Xing, Y., Liu, B., 2009a. New exact solutions for free vibrations of rectangular thin plates by symplectic dual method. *Acta Mechanica Sinica* 25, 265–270. doi:10.1007/s10409-008-0208-4.
- [26] Xing, Y., Sun, Q., Liu, B., Wang, Z., 2018. The overall assessment of closed-form solution methods for free vibrations of rectangular thin

- 502 plates. International Journal of Mechanical Sciences 140, 455–470.
503 doi:10.1016/j.ijmecsci.2018.03.013.
- 504 [27] Xing, Y., Wang, Z., 2020a. An extended separation-of-variable method
505 for the free vibration of orthotropic rectangular thin plates. International
506 Journal of Mechanical Sciences 182, 105739. doi:10.1016/j.ijmecsci.
507 2020.105739.
- 508 [28] Xing, Y., Wang, Z., 2020b. An improved separation-of-variable method
509 for the free vibration of orthotropic rectangular thin plates. Composite
510 Structures 252, 112664. doi:10.1016/j.compstruct.2020.112664.
- 511 [29] Xing, Y.F., Liu, B., 2009b. New exact solutions for free vibrations of
512 thin orthotropic rectangular plates. Composite Structures 89, 567–574.
513 doi:10.1016/j.compstruct.2008.11.010.
- 514 [30] Yuan, S., Ye, K., Williams, F., 2004. Second order mode-finding method
515 in dynamic stiffness matrix methods. Journal of Sound and Vibration
516 269, 689–708. doi:10.1016/S0022-460X(03)00126-3.
- 517 [31] Zhang, S., Xu, L., Li, R., 2019. New exact series solutions for transverse
518 vibration of rotationally-restrained orthotropic plates. Applied Mathe-
519 matical Modelling 65, 348–360. doi:10.1016/j.apm.2018.08.033.
- 520 [32] Zhong, W.X., 1995. A new systematic methodology for theory of elas-
521 ticity. Dalian University of Technology Press, Dalian , 182–187.
- 522 [33] Zhong, Y., Zhao, X.F., Li, R., 2013. Free vibration analysis of rectangu-
523 lar cantilever plates by finite integral transform method. International
524 Journal for Computational Methods in Engineering Science and Me-
525 chanics 14, 221–226. doi:10.1080/15502287.2012.711424.